Acute and Consolidation Transcriptional Programs in the Central Amygdala Following Parabrachial Pain-circuit Activation

Andrew Pelos

A thesis

submitted in partial fulfillment of the

requirements for the degree of

Master of Science

University of Washington

2026

Committee:

Richard Palmiter

Garret Stuber

Sekun Park

Program Authorized to Offer Degree:

Neuroscience

University of Washington

Abstract

Acute and Consolidation Transcriptional Programs in the Central Amygdala Following Parabrachial Pain-circuit Activation

Andrew Pelos

Chair of the Supervisory Committee:

Richard Palmiter

Department of Biochemistry

The central nucleus of the amygdala (CeA) receives nociceptive input from parabrachial nucleus (PBN) neurons expressing the CGRP precursor encoded by the *Calca* gene, and plasticity at this synapse has been implicated in chronic pain development. Which CeA populations respond to parabrachial input, and how their transcriptional programs evolve from acute activation to consolidation, remains unclear. Here, we used single-cell RNA sequencing to characterize CeA GABAergic neuron responses after chemogenetic activation of *Calca*^{PBN} neurons at acute (D0.01, 30 minutes) and consolidation (D3, 3 days) timepoints. Analysis of 19,544 neurons resolved 21 clusters including 13 core CeA populations. Acute activation preferentially engaged C9, a population co-expressing *Prkcd* and *Calcrl*, which showed significant upregulation of immediate early genes including *Arc*, *Egr1*, and *Egr4*. Differential expression analysis revealed striking temporal asymmetry: D0.01 showed 1,872 differentially expressed genes (DEGs) with balanced directionality, while D3 showed 4,787 DEGs with a 25-fold bias toward downregulation. Suppressed genes included ionotropic receptors (*Gria4*, *Gabra1*), postsynaptic scaffolds (*Camk2b*, *Shank3*, *Homer2*), and the transcription factor *Foxo3*. Temporal overlap was minimal: just 15 genes sustained significance in C8 (*Calcrl* neurons) across both timepoints. Gene ontology analysis showed 87% of enriched terms were D3-specific, including synaptic plasticity regulation and negative regulation of long-term potentiation. These findings demonstrate that acute activation and early consolidation engage distinct transcriptional programs, with consolidation characterized by widespread suppression consistent with homeostatic refinement rather than simple potentiation. This molecular taxonomy identifies specific CeA populations and gene programs as potential intervention targets in the transition from acute to nociplastic pain.

Acknowledgments

I am deeply grateful to my thesis committee: Dr. Richard Palmiter, Dr. Garret Stuber, and Dr. Sekun Park, for their mentorship, patience, and grace throughout this project. Their guidance shaped both my scientific thinking and my growth as a researcher.

This work would not have been possible without the efforts of many individuals. I thank Sekun Park for designing the experimental paradigm and preparing the sequencing libraries, Sekun Park and Jane Chen for preparing and dissecting the tissue samples, and Rachel Felix for testing the mice for CNO response. Sequencing was performed at the Fred Hutchinson Cancer Research Center Genomics Core. This research was supported by the Howard Hughes Medical Institute (HHMI).

I. Literature Review and Rationale

Chronic pain is a heterogeneous clinical condition defined by persistent pain that outlasts normal tissue healing, often accompanied by substantial affective and cognitive burden (Fitzcharles et al., 2021; Kuner & Kuner, 2021). A growing body of work emphasizes that many chronic pain states are maintained by maladaptive central processing rather than ongoing peripheral injury. "Central sensitization" refers specifically to increased responsiveness of nociceptive neurons in the central nervous system, including activity-dependent plasticity in the spinal dorsal horn that amplifies nociceptive transmission to the brain (Latremoliere & Woolf, 2009; Woolf, 2011). More recently, the clinical descriptor "nociplastic pain" was introduced to categorize pain arising from altered nociceptive function without clear evidence of tissue damage or somatosensory nerve lesion; it is distinct from nociceptive pain (tissue injury) and neuropathic pain (nerve lesion) (Fitzcharles et al., 2021; Kosek et al., 2016; Palmiter, 2024). While central sensitization at spinal levels contributes to nociplastic pain, the full syndrome implicates durable plasticity

across distributed brain circuits integrating nociception with affect, arousal, and defensive behavior (Kuner & Kuner, 2021; Palmiter, 2024). Nociplastic pain is characterized by diffuse allodynia, hyperalgesia, and frequent comorbidity with anxiety, depression, and fatigue. These features that are difficult to explain by spinal mechanisms alone and suggest supraspinal circuit reorganization (Palmiter, 2024).

Recent work from our laboratory converges on a small population of parabrachial nucleus (PBN) neurons expressing *Calca*, the gene encoding the alpha subunit of calcitonin gene-related peptide (CGRP), as an upstream driver of nociplasticity. *Calca*^{PBN} neurons constitute a major component of the spino-parabrachio-amygdaloid pathway and serve as a threat-activated relay that transmits diverse aversive signals, including nociceptive, visceral, and pruriceptive stimuli, to forebrain structures (Kuner & Kuner, 2021; Palmiter, 2018; Pauli et al., 2022). *Calca* neurons reside primarily within the external lateral PBN (PBle) and constitute one of approximately 21 molecularly defined neuronal subclusters identified through single-cell RNA sequencing of PBN tissue (Pauli et al., 2022). These neurons project their axons via the central tegmental tract to forebrain targets including the CeA and the bed nucleus of the stria terminalis (BNST), distinct from ventral pathway populations such as *Pdyn*-expressing neurons that preferentially target hypothalamic structures (Pauli et al., 2022). Notably, *Calca* neurons are glutamatergic and some co-express *Chat* (indicating cholinergic capacity), and molecular profiling reveals at least two *Calca* subclusters that differ in transcription factor expression and may have distinct functional properties (Pauli et al., 2022). This molecular heterogeneity within the *Calca* population raises the possibility that different *Calca* neuron subtypes may contribute differentially to the nociplastic phenotype, though this has not been tested directly. Calcium imaging studies demonstrate that many *Calca*^{PBN} neurons respond to diverse threat modalities, suggesting they

encode aversive salience rather than stimulus-specific information (Campos et al., 2018; Chen et al., 2018; Park et al., 2024). Preventing neurotransmitter release from *Calca*^{PBN} neurons blocks both the manifestation and maintenance of persistent allodynia across multiple models, while chemogenetic activation of these neurons is sufficient to induce long-lasting allodynia (3-4 days at a single activation and ~14 days after three consecutive activations) that scales with the duration and intensity of stimulation (Condon et al., 2024). Notably, CGRP itself is not required for allodynia in at least one neuropathic context, indicating that *Calca*-lineage neurons can drive nociplasticity through glutamatergic or other non-CGRP signaling (Condon et al., 2024).

Among forebrain structures, the CeA occupies a strategic position for coupling ascending nociceptive and interoceptive signals to emotional learning and descending modulation of pain (Kuner & Kuner, 2021; Mazzitelli et al., 2021; Presto & Neugebauer, 2022). The CeA is a principal target of *Calca*^{PBN} projections and is positioned to translate parabrachial threat signals into durable affective and autonomic states (Kato et al., 2018; Palmiter, 2018; Pauli et al., 2022). At PBN→CeA synapses, CGRP released from parabrachial terminals enhances postsynaptic responsiveness and facilitates synaptic potentiation (J. S. Han et al., 2005; Presto & Neugebauer, 2022). Brief nociceptive stimulation is sufficient to induce lasting synaptic strengthening at this synapse, with potentiation developing and persisting for ~3 days after the stimulus ends (Kissiwaa & Bagley, 2018). Chronic pain models additionally show structural remodeling of PBN-CeA synaptic architecture through trans-synaptic signaling mechanisms (Gandhi et al., 2021). These observations support a temporal framework in which early activity-dependent plasticity is followed by consolidation of synaptic and cellular phenotypes over subsequent days (Gandhi et al., 2021; Kato et al., 2018; Kissiwaa & Bagley, 2018).

Dissecting these processes requires resolving the pronounced cellular heterogeneity of the CeA. The region is dominated by GABAergic neurons with striatal-like developmental origins, but these neurons partition into numerous transcriptionally defined subtypes with distinct projection patterns, electrophysiological properties, and behavioral roles (Sah et al., 2003; Swanson & Petrovich, 1998; Wang et al., 2023). Recent single-cell atlases have defined this molecular diversity, identifying over a dozen distinct neuronal populations with validated differences in spatial distribution and long-range connectivity (O'Leary et al., 2022; Wang et al., 2023). Complementary work has linked transcriptional cell states to behavioral learning and memory consolidation, revealing that activity-dependent gene programs are engaged in cell-type specific patterns (Hochgerner et al., 2023; Yeh et al., 2024; Yu et al., 2023). However, which specific CeA populations respond transcriptionally to parabrachial nociceptive input, and how these programs evolve from acute activation to sustained plasticity, remains incompletely understood.

Filling this gap is essential for understanding CeA contributions to nociplastic pain and for identifying potential novel therapeutic targets. Doing so requires integrating circuit-level understanding of CeA organization, molecular definitions of CeA cell types, and knowledge of the synaptic and neuromodulatory mechanisms through which parabrachial input shapes CeA function. The following sections review these topics in detail. I then present a single-cell RNA sequencing study designed to identify the specific CeA populations and gene programs engaged by chemogenetic activation of parabrachial *Calca* neurons across acute and early consolidation timepoints.

Anatomical Organization of the CeA and Classical Circuitry

The central nucleus of the amygdala (CeA) differs fundamentally from the adjacent basolateral amygdala (BLA) in both developmental origin and cellular composition. Whereas BLA neurons derive from pallial (cortical) progenitors and are predominantly glutamatergic, CeA neurons arise from subpallial ganglionic eminence territories that also give rise to the striatum (Sah et al., 2003; Swanson & Petrovich, 1998). This shared developmental lineage is reflected in the neurochemical and electrophysiological properties of CeA neurons: like striatal medium spiny neurons, CeA projection neurons are GABAergic, express markers such as *Ppp1r1b*, and exhibit similar membrane properties and dopamine receptor expression patterns (Kim et al., 2017; Sah et al., 2003; Swanson & Petrovich, 1998). This organizational principle positions the CeA not as a cortical-like associative structure, but as a specialized output gate analogous to the striatum's role in motor circuits, which selectively permits or suppresses signals to downstream effector systems.

The CeA is classically subdivided into three major domains based on cytoarchitecture and connectivity: the capsular (CeC), lateral (CeL), and medial (CeM) subdivisions (Pitkänen et al., 1997; Sah et al., 2003). These subdivisions occupy distinct positions along the mediolateral axis and differ in their input-output relationships. The CeC lies at the far lateral edge of the nucleus and receives particularly dense innervation from the PBN, earning it the designation “nociceptive amygdala” in some literature (Sah et al., 2003; Wang et al., 2023). The CeL occupies an intermediate position and serves as a critical site for local circuit processing, receiving convergent inputs from multiple sources and housing inhibitory microcircuits that regulate CeM output (Ciocchi et al., 2010; Haubensak et al., 2010). The CeM constitutes the principal output division, sending long-range projections to brainstem and hypothalamic targets

that execute autonomic, endocrine, and behavioral components of emotional responses (LeDoux et al., 1988; Sah et al., 2003).

The CeA receives convergent afferent input from brain regions carrying complementary information relevant to threat assessment and internal state monitoring. The BLA provides learned stimulus-outcome associations, transmitting information about conditioned cues that predict danger or reward (Kim et al., 2017; Pitkänen et al., 1997). The PBN, as discussed, conveys signals ascending from the spinal cord and viscera, representing the primary route through which bodily threat information reaches the amygdala (LeDoux et al., 1988; Sah et al., 2003). Additional inputs arrive from insular and prefrontal cortices, which likely contribute contextual and cognitive information, and from hypothalamic and brainstem nuclei relaying autonomic and arousal states (Pitkänen et al., 1997; Rizvi et al., 1991). Anatomical tracing studies established that these inputs are not uniformly distributed: BLA projections target primarily CeL and CeM, whereas parabrachial projections preferentially innervate CeC and lateral portions of CeL (Pitkänen et al., 1997; Sah et al., 2003). This anatomical segregation provides a substrate for parallel processing of distinct information streams within the CeA.

Efferent projections from the CeA target a distributed network of brainstem, hypothalamic, and forebrain structures that mediate distinct components of emotional and defensive responses. Discrete CeA output pathways control separable aspects of conditioned fear: projections to the lateral hypothalamus mediate conditioned cardiovascular responses, whereas projections to the periaqueductal gray (PAG) contribute to freezing and other defensive behaviors (LeDoux et al., 1988). CeA projections to the PAG are topographically organized, engaging specific longitudinal PAG columns associated with distinct defensive response patterns (Rizvi et al., 1991). Additional major targets include the BNST, which supports sustained

anxiety-like states, and brainstem nuclei controlling respiration, startle, and hormonal release (Hitchcock & Davis, 1991; LeDoux et al., 1988). The CeA also projects back to the PBN, forming a reciprocal loop that can modulate ascending nociceptive gain (Wang et al., 2023). Beyond these descending and hypothalamic targets, a distinct population of CRH-expressing GABAergic neurons in the CeA projects to the ventral tegmental area (VTA). These VTA-projecting neurons are largely negative for both *Prkcd* and *Sst*, distinguishing them from the populations that dominate local CeL microcircuits and descending brainstem projections (Dedic et al., 2018). This pathway acts on CRHR1-expressing dopamine neurons to positively modulate dopamine release, and chronic depletion of CRH from these projection neurons increases anxiety-like behavior (Dedic et al., 2018). The CeA thus influences not only defensive responses through brainstem targets, but also motivational state through access to mesolimbic dopamine systems. This distributed output architecture enables the CeA to orchestrate coordinated emotional responses spanning behavioral, autonomic, and endocrine domains.

Within the CeL, behaviorally consequential computations emerge from interactions between molecularly distinct inhibitory populations. Two functionally separable neuron populations in CeL exhibit opposite responses during fear conditioning: CeL_{on} neurons increase firing to conditioned stimuli, while CeL_{off} neurons, which largely correspond to *Prkcd*-expressing neurons (encoding PKCδ), are inhibited (Ciocchi et al., 2010; Haubensak et al., 2010). Both populations send inhibitory projections to CeM output neurons, but their reciprocal inhibitory connections create a competitive microcircuit architecture. Pharmacological inactivation of CeL induces freezing behavior by releasing CeM from tonic inhibition, whereas inactivation during conditioning impairs fear acquisition, indicating that plasticity within CeL is necessary for learning (Ciocchi et al., 2010). Silencing $PKC\delta^+$ neurons enhances conditioned

freezing, consistent with their role as inhibitory gatekeepers of CeM output (Haubensak et al., 2010). Somatostatin-expressing (*Sst*$^{+}$) neurons in CeL serve as a key counterpart to PKCδ^{+} neurons: they undergo synaptic potentiation during fear conditioning, can drive freezing when activated, and exert inhibitory control over PKCδ^{+} neurons, thereby disinhibiting CeM (Fadok et al., 2017; Yeh et al., 2024). This reciprocal inhibitory organization, sometimes likened to the direct and indirect pathways of the basal ganglia, allows the CeA to flexibly switch between behavioral states depending on which population dominates (Kim et al., 2017). However, this analogy does not extend cleanly to output projections: unlike striatal direct and indirect pathway neurons, which define segregated output channels, CeL *Prkcd* neurons function primarily as local circuit elements with limited long-range projections, whereas *Sst* neurons, particularly the MC-3 subtype lacking *Vipr2* and *Crh* co-expression, constitute the major descending projection from CeL to brainstem targets including the PBN, PAG, and substantia nigra (Wang et al., 2023).

This microcircuit framework extends beyond fear to encompass appetitive behavior and valence coding more broadly. Genetically defined BLA→CeA pathways can promote or suppress reward-seeking behavior through parallel circuits resembling basal ganglia direct and indirect pathways: BLA *Ppp1r1b* neurons project to dopamine D1 receptor-expressing CeA neurons to promote appetitive behavior, whereas BLA *Rspo2* neurons project to D2 receptor-expressing CeA neurons to suppress it (Kim et al., 2017). This functional parallel reinforces the conceptual link between CeA and striatal organization and suggests that the competitive inhibitory architecture of the CeA may have evolved as a general mechanism for selecting among alternative behavioral responses to motivationally significant stimuli, whether aversive or appetitive.

CeA in Pain Processing

The anatomical and circuit organization described above positions the CeA as a central hub for pain processing, but understanding its role in nociception requires examining how specific CeA populations respond to painful stimuli and how these responses change in chronic pain states. The CeA contributes to both sensory-discriminative and affective-motivational dimensions of pain, integrating ascending nociceptive information with learned associations and internal states to generate appropriate behavioral and autonomic responses (Kuner & Kuner, 2021; Neugebauer et al., 2004).

At PBN-to-CeA synapses, CGRP acts as a neuromodulator that enhances postsynaptic responsiveness through NMDA- and PKA-dependent mechanisms, amplifying the impact of nociceptive input on CeA neuron activity (J. S. Han et al., 2005; Presto & Neugebauer, 2022). Brief nociceptive stimulation induces input-specific synaptic potentiation reflected by an increased AMPAR/NMDAR current ratio that develops over one day and persists for at least three days before returning to baseline (Kissiwaa & Bagley, 2018). This potentiation involves a biphasic change in AMPA receptor subunit composition: GluA2-lacking (calcium-permeable) receptors are transiently incorporated postsynaptically at PBN-CeA synapses during the first day, as evidenced by increased inward rectification that normalizes by day three even while overall potentiation persists (Kissiwaa & Bagley, 2018). The transient switch to calcium-permeable receptors creates conditions for priming: if a second nociceptive stimulus occurs during this vulnerability window (approximately day 1-2), potentiation persists beyond seven days rather than returning to baseline, substantially prolonging enhancement of nociceptive transmission through the amygdala (Kissiwaa & Bagley, 2018). This mechanism suggests that repeated

noxious input during vulnerability windows can produce cumulative, prolonged sensitization of the PBN→CeA pathway.

Chronic pain models further implicate structural remodeling at PBN-CeA synapses. The structural organization of these synapses depends on trans-synaptic signaling through the GluD1-cerebellin 1 (Cbln1) complex, which exhibits remarkable input- and cell-type specificity. GluD1 is expressed postsynaptically at axo-somatic and punctate locations specifically on PKCδ$^+$ neurons in the CeLC, with minimal expression on somatostatin neurons (Gandhi et al., 2021). This GluD1 expression shows preferential localization to vGluT2$^+$ (parabrachial) terminals rather than vGluT1$^+$ (BLA) terminals, indicating synapse-specific organization (Gandhi et al., 2021). Cbln1 is expressed presynaptically by PBN neurons and released to bind GluD1, forming a tripartite complex with presynaptic neurexin that maintains synaptic structure (Gandhi et al., 2021). In both inflammatory and neuropathic pain models, GluD1 (*Grid1*) and *Cbln1* are downregulated while AMPA receptor expression increases, a pattern more pronounced in the right CeA, consistent with hemispheric lateralization of pain-related plasticity (Allen et al., 2021; Gandhi et al., 2021). Importantly, a single infusion of recombinant Cbln1 into the CeA produced sustained (>1 week) reversal of mechanical hypersensitivity and normalized CeA neuron hyperexcitability through a GluD1-dependent mechanism (Gandhi et al., 2021). These observations collectively support a temporal framework in which early activity-dependent receptor trafficking is followed by structural reorganization of synaptic architecture over subsequent days (Gandhi et al., 2021; Kato et al., 2018; Kissiwaa & Bagley, 2018).

The CeC receives the densest innervation from parabrachial CGRP$^+$ fibers and expresses high levels of the CGRP receptor component *Calcrl*, positioning it as the primary entry point for ascending nociceptive information from the PBN into the amygdala (S. Han et al., 2015; Kuner

& Kuner, 2021; Wang et al., 2023). *Calcrl*-expressing neurons in CeC and lateral CeL are direct postsynaptic targets of parabrachial *Calca* terminals and show robust activation following noxious stimulation (Campos et al., 2018; Chen et al., 2018). However, *Calcrl* expression is not restricted to a single molecularly defined population; it marks subsets of both *Prkcd* neurons in posterior CeA and *Cyp26b1* neurons in anterior CeA, suggesting that parabrachial nociceptive input engages multiple CeA cell types with potentially distinct downstream functions (Bowen et al., 2020; Wang et al., 2023).

The CeA actively modulates pain perception through bidirectional control mechanisms that depend on the balance between molecularly distinct populations. *Prkcd*-expressing neurons and *Sst*-expressing neurons exert opposing influences on nociception: *Prkcd* neurons are generally pro-nociceptive while *Sst* neurons are generally anti-nociceptive (Wilson et al., 2019). Both populations receive direct monosynaptic input from the PBN, positioning them to respond to ascending nociceptive signals with opposite behavioral consequences (Wilson et al., 2019). *Prkcd*-expressing neurons and somatostatin-expressing neurons exert opposing influences on nociception: *Prkcd* neurons are generally pro-nociceptive while *Sst* neurons are generally anti-nociceptive (Wilson et al., 2019). Both populations receive direct monosynaptic input from the PBN, positioning them to respond to ascending nociceptive signals with opposite behavioral consequences (Wilson et al., 2019). Following nerve injury, acute-phase studies report increased excitability in *Prkcd* neurons and decreased activity in *Sst* neurons, shifting the balance toward enhanced nociception (Wilson et al., 2019). However, this pattern may not persist into chronic pain states: Kiritoshi et al. (2024) found that neither *Prkcd* nor *Calcrl* neurons showed significant hyperexcitability at chronic timepoints, while only a subset of regular-spiking *Sst* neurons exhibited increased excitability, yet chemogenetic inhibition of *Sst* neurons did not measurably

affect chronic pain behaviors. This dissociation between cellular hyperexcitability and behavioral relevance suggests that the circuit logic governing chronic pain may differ fundamentally from that established in acute models (Kiritoshi et al., 2024).

A third population, neurons expressing corticotropin-releasing hormone (CRH), contributes specifically to the affective-motivational dimension of pain. *Crh* neurons in the CeA are largely distinct from both *Prkcd* and *Sst* populations and function as a gain-control mechanism that amplifies responses to ambiguous or weak threats that might otherwise be ignored (Sanford et al., 2017). This gain function extends to pain processing: optogenetic silencing of CeA *Crh* neurons reduces emotional-affective pain behaviors, including audible and ultrasonic vocalizations, in both acute inflammatory and chronic neuropathic pain models without altering mechanical sensitivity thresholds, while optogenetic activation induces anxiety-like responses and affective pain behaviors in uninjured animals (Mazzitelli et al., 2021). *Crh* neurons thus appear to specifically amplify pain's emotional impact rather than sensory intensity. Importantly, CRH and non-CRH populations show distinct temporal profiles of plasticity during pain chronification: *Crh* projection neurons exhibit hyperexcitability with concurrent PBN→CeA synaptic potentiation during the acute phase (1 week post-injury), but at chronic timepoints (4 weeks) this hyperexcitability shifts to non- *Crh* populations and occurs without accompanying synaptic plasticity at PBN inputs (Kiritoshi et al., 2024). This temporal dissociation suggests that the cellular substrates initiating pain sensitization may differ fundamentally from those maintaining chronic pain states, with *Crh* neurons driving the acute transition while the identity of populations sustaining the chronic condition remains unclear. Notably, Kiritoshi et al. (2024) found chronic-phase hyperexcitability in a subset of *Sst* rather than *Prkcd* neurons, though

chemogenetic inhibition of neither population significantly affected chronic pain behaviors (Kiritoshi et al., 2024).

A critical but often overlooked component of this circuitry is the inhibitory feedback pathway from CeA to the PBN. The molecular composition of this descending projection reveals a heterogeneous population: around 42% of retrogradely-labeled CeA neurons projecting to PBN express dynorphin, 26% express somatostatin, and 9% express *Crh*, with some neurons co-expressing multiple markers (Raver et al., 2020). The PBN itself contains very few GABAergic interneurons, making CeA the primary source of inhibitory control over these nociceptive relay neurons (Raver et al., 2020). This descending pathway functions as a brake on ascending nociceptive signaling: optogenetic activation of CeA→PBN terminals suppresses both acute and chronic pain behaviors, while optogenetic inhibition in naive animals is sufficient to evoke pain-like responses, establishing bidirectional causality for this descending control mechanism (Raver et al., 2020). In chronic pain states following nerve injury, this inhibitory input weakens substantially: optogenetically evoked inhibitory currents in PBN neurons are approximately five-fold smaller in injured animals compared to controls, and the frequency of miniature inhibitory postsynaptic currents is reduced by roughly 50% (Raver et al., 2020). Notably, *Crh* -expressing CeA terminals in PBN are sufficient to produce analgesia when selectively activated, suggesting that specific molecular subtypes within the feedback pathway may be particularly important for pain modulation (Raver et al., 2020). These findings demonstrate that chronic pain involves not only sensitization of ascending pathways but also active failure of descending inhibitory control, creating conditions for a feedforward loop that sustains the pain state.

The reciprocal PBN↔CeA circuit thus operates as an integrated system where dysfunction at either node can propagate to the other. Hyperactivity of parabrachial *Calca*

neurons drives CeA plasticity, recruiting *Crh* neurons acutely and shifting the *Prkcd/Sst* balance toward pro-nociceptive output, while weakened CeA→PBN inhibition further releases parabrachial neurons from constraint, increasing the ascending nociceptive drive that initiated the cascade (Kiritoshi et al., 2024; Kuner & Kuner, 2021; Raver et al., 2020). Interrupting this cycle, either by silencing parabrachial *Calca* neurons or by restoring CeA inhibitory output, can reverse established chronic pain phenotypes, suggesting that the circuit maintains chronic pain through ongoing activity rather than irreversible structural damage (Condon et al., 2024; Raver et al., 2020).

Recent work examining how parabrachial activation transforms amygdala representations provides mechanistic insight into this circuit plasticity. Zimmerman et al. (2025) demonstrated that optogenetic stimulation of parabrachial *Calca* neurons selectively reactivates neural representations of recently consumed novel stimuli in the CeA, even when stimulation occurs 30 minutes after the initial experience (Zimmerman et al., 2023). This postingestive reactivation was time-locked to individual bouts of *Calca* neuron stimulation and predicted subsequent strengthening of stimulus representations upon memory retrieval. Critically, novel stimuli triggered sustained PKA activity in CEA neurons, potentially providing a biochemical eligibility trace that marks recently activated neurons for preferential reactivation by delayed CGRP input (Zimmerman et al., 2023). These findings suggest that parabrachial CGRP signaling does not simply activate CeA neurons but actively shapes which representations are stabilized versus degraded, providing a mechanism by which the PBN→CeA pathway could selectively consolidate pain-related memories.

CeA pain processing also exhibits hemispheric lateralization, though the generalizability of this phenomenon across pain modalities requires careful consideration. In bladder pain

models, optogenetic activation of parabrachial *Calca* terminals in the right CeA promotes hyperalgesia while identical stimulation in the left CeA produces antihyperalgesia (Allen et al., 2023). Notably, bath application of CGRP to acute slices increases action potential firing in CeA neurons from both hemispheres, indicating that the opposing behavioral outcomes do not arise from lateralized sensitivity to the peptide but rather from differences in downstream circuit organization (Allen et al., 2023). In naive animals, the left CeA's analgesic influence predominates, but this protective effect diminishes following bladder sensitization, potentially due to reduced CGRP signaling in the left hemisphere (Allen et al., 2023). Whether similar hemispheric specialization applies to somatic pain modalities remains unclear; the Allen et al. findings derive specifically from visceral pain models using optogenetic terminal stimulation in CeA rather than somatic activation of PBN neurons. The present study employs unilateral stimulation of right-hemisphere parabrachial *Calca* cell bodies, which project bilaterally to CeA albeit with a strong ipsilateral bias. This design provides an opportunity to examine whether transcriptomic responses differ between ipsilateral and contralateral CeA, potentially revealing molecular correlates of lateralized pain processing.

Molecular Heterogeneity of CeA Neurons

The functional populations described above, particularly *Prkcd, Calcrl*, *Sst*, and *Crh* neurons, represent operational categories historically defined by single marker genes and their associated behavioral phenotypes. Single-cell transcriptomic studies reveal, however, that the true molecular organization of the CeA is considerably more complex: each marker labels multiple transcriptionally distinct subtypes that differ in spatial distribution, projection targets, neuromodulatory receptor expression, and likely function. Resolving which specific subtypes

respond to parabrachial input and undergo plasticity during pain chronification requires methods that can distinguish these populations at higher resolution than marker gene approaches permit.

Recent single-cell atlases organize CeA GABAergic neurons into two broad classes primarily distinguished by expression of *Ppp1r1b* (Class 1) versus its absence (Class 2), with *Nefm* marking many Class 2 neurons. This two-class framework represents only the highest level of a hierarchical taxonomy containing at least 13 transcriptionally distinct neuronal populations (Wang et al., 2023). Within Class 1, somatostatin-expressing neurons partition into at least two populations with dramatically different connectivity despite their shared *Sst* expression. One subtype (corresponding to molecular cluster MC-2 in this study) co-expresses *Vipr2*, *Crh*, *Tac2*, and *Nts*, is restricted to posterior and medial CeL, and shows minimal long-range projections. The other (MC-3) lacks these markers, spans anterior through posterior CeC and CeL, and constitutes the major descending projection to PBN, ventrolateral PAG, substantia nigra, and parvocellular reticular formation (Wang et al., 2023). These populations are spatially intermingled and cannot be distinguished by *Sst* immunohistochemistry or *Sst*-Cre driver lines, yet show approximately 11-fold differences in probability of projecting to descending targets (Wang et al., 2023). This heterogeneity within classically defined "*Sst* neurons" likely explains contradictory reports on their behavioral roles, i.e., outcomes depend on which molecular subtype predominates in any given manipulation.

Similar complexity exists within PKCδ-expressing populations. *Prkcd* marks subsets of both the anterior *Cyp26b1*$^{+}$/*Crym*$^{+}$ population (MC-10, corresponding to seq-c6) and the posterior *Cartpt*$^{+}$ population (MC-6, corresponding to seq-c8), which occupy largely non-overlapping CeA territories (Wang et al., 2023). The posterior population shows higher *Prkcd* expression levels and stronger *Cartpt* co-expression, while the anterior population co-expresses

Penk and shows lower *Ppp1r1b* levels. Both populations include neurons that project to the BNST, but neither constitutes the majority of this projection class (Wang et al., 2023). Whether these anterior and posterior *Prkcd* subtypes play equivalent roles in pain modulation, or whether one predominates in the sensitization described by Wilson et al. (2019), remains unknown.

Additional populations identified through unbiased transcriptomics do not map cleanly onto the *Prkcd*/*Sst*/*Crh* framework derived from functional studies. O'Leary et al. (2022) identified *Nr2f2*-expressing and *Isl1*-expressing populations that together comprise approximately one-third of CeA neurons yet were unresolved in earlier classifications. *Isl1*$^{+}$ neurons occupy the medial CeA, show molecular and spatial similarity to striatal direct-pathway neurons, and constitute a major long-range projecting population targeting substantia nigra, PAG, and PBN (O'Leary et al., 2022). *Nr2f2*$^{+}$ neurons occupy a transitional zone between medial and lateral CeA, project preferentially to the lateral hypothalamus, and may represent a functionally distinct population that has resisted characterization precisely because it lacks the canonical markers used in most studies (O'Leary et al., 2022). How these populations respond to nociceptive input is unexplored.

The *Crh* population introduced previously also exhibits internal molecular heterogeneity that has functional consequences. A substantial fraction of CeA *Crh* neurons co-express prodynorphin (*Pdyn*), and these co-expressing neurons engage distinct signaling pathways with different behavioral outcomes: GABA release from *Crh* neurons regulates baseline anxiety states, whereas CRH and dynorphin peptide release specifically mediates responses to learned threats and chemogenetically induced anxiety (Pomrenze et al., 2019). The dynorphin/kappa-opioid receptor (KOR) system provides an additional layer of modulation: KOR activation decreases feedforward inhibitory transmission onto *Crh* neurons at PBN→CeA synapses,

effectively disinhibiting CRH output and enhancing affective pain responses without altering mechanosensory thresholds (Hein et al., 2021). This positions dynorphin-KOR signaling as a presynaptic gate that controls CRH-mediated amplification of aversive states. In neuropathic pain models, KOR antagonism in the right (but not left) CeA restores diffuse noxious inhibitory controls while leaving baseline sensory thresholds intact, indicating that KOR signaling specifically impairs descending inhibition rather than directly driving hypersensitivity (Phelps et al., 2019). This circuit mechanism (dynorphin gating CRH output) may represent a key node where nociplastic states are initiated or maintained.

Beyond static molecular identity, CeA neurons exhibit dynamic activity-dependent transcriptional states that evolve over time. During fear learning, only a sparse subset of neurons within each molecularly defined population upregulates immediate early genes (IEGs) such as *Fos*, *Arc*, and *Nr4a1*, consistent with the sparse encoding characteristic of memory engrams (Hochgerner et al., 2023). Critically, no single IEG reliably marks all activated neurons at every timepoint; rather, a consensus panel of activity-regulated genes better captures the full spectrum of neuronal activation (Hochgerner et al., 2023). These IEG-high cells show coordinated upregulation of genes involved in synaptic signaling, plasticity, neurite outgrowth, and development, programs that extend beyond immediate activity markers into consolidation-related transcriptional cascades that persist for at least 24 hours (Hochgerner et al., 2023). Notably, the IEG response was restricted to specific cell types: among CeA GABAergic neurons, two *Prkcd* subtypes (GABA-9 and GABA-16) showed particularly strong transcriptional responses to fear conditioning, while other subtypes showed minimal activation (Hochgerner et al., 2023). This cell-type specificity of activity-dependent transcription suggests that even within populations

sharing a marker gene, only certain subtypes participate in any given behavioral or physiological response.

Whether similar sparse, subtype-specific transcriptional responses occur following parabrachial activation can be addressed through single-cell approaches. The temporal framework established by Kiritoshi et al. (2024), acute CRH-neuron involvement followed by chronic non-CRH plasticity, predicts that transcriptomic profiling at different timepoints should reveal shifting cellular substrates (Kiritoshi et al., 2024). Early timepoints may show IEG responses concentrated in CRF-expressing subtypes and their immediate targets, while later timepoints may reveal sustained transcriptional changes in *Prkcd* or other non-CRH populations. The present study's D0.01 versus D3 design is positioned to capture this transition, with D0.01 reflecting the immediate transcriptional response to PBN activation and D3 capturing early consolidation that may presage the chronic state.

Finally, the translational relevance of these molecular distinctions is supported by cross-species transcriptomic comparisons. The CeA emerges as the most evolutionarily conserved subdivision of the amygdala, with remarkably preserved cell type composition across mouse, macaque, and human (Yu et al., 2023). Human homologs of mouse *Prkcd*, *Sst*, and *Tac2* populations maintain similar gene expression signatures and spatial organization within the CeA, and the neuropeptide systems implicated in pain modulation, including CRH, dynorphin, and somatostatin, show conserved expression patterns across primates (Yu et al., 2023). This conservation implies that the transcriptional logic of cell-type specific plasticity defined in the mouse CeA is likely to inform understanding of human chronic pain circuitry. Characterizing cell-type specific transcriptional responses to parabrachial activation and their temporal

dynamics across the transition from acute response to early consolidation thus asks questions with direct relevance to the neural substrates of human nociplastic pain.

Study Design & Rationale

To address these questions, the present study employs single-cell RNA sequencing of fixed CeA tissue following chemogenetic activation of parabrachial *Calca* neurons. This experimental approach was chosen for several reasons. First, work from our laboratory established that chemogenetic activation of *Calca* neurons via hM3Dq-DREADD plus CNO activation is sufficient to induce persistent mechanical allodynia lasting 3-4 days depending on stimulation parameters, recapitulating a key behavioral feature of nociplastic pain without requiring tissue injury or nerve lesion (Condon et al., 2024). This sufficiency is critical: it isolates parabrachial drive as the causal variable and eliminates peripheral confounds such as ongoing inflammation, immune cell infiltration, or Wallerian degeneration that accompany injury-based models. The clean separation of brain from spinal and peripheral contributions allows any transcriptomic changes observed in CeA neurons to be attributed specifically to parabrachial activation rather than to systemic or local inflammatory signaling that might independently affect amygdala gene expression.

Second, chemogenetic activation provides controllable stimulation parameters that can be calibrated to produce reliable behavioral outcomes. Condon et al. (2024) demonstrated that allodynia duration scales with both the intensity and duration of *Calca* neuron activation, indicating that this population encodes a graded signal that determines the magnitude of downstream plasticity (Condon et al., 2024). For the present study, stimulation parameters were selected to reliably induce allodynia persisting beyond the D3 collection timepoint, ensuring that

transcriptomic profiling captures a physiologically relevant state rather than a subthreshold perturbation. However, an important caveat must be acknowledged: chemogenetic activation produces sustained, relatively synchronous depolarization of the targeted population, which may differ in temporal dynamics, co-release patterns, or downstream signaling from the phasic, stimulus-locked firing that characterizes naturalistic nociceptive responses. Whether transcriptomic programs induced by chemogenetic activation fully recapitulate those engaged by peripheral injury remains an open question that the present study cannot directly address, though convergence between our findings and those from injury-based models would strengthen confidence in their generalizability.

The selection of D0.01 and D3 timepoints was motivated by converging evidence from synaptic plasticity studies and behavioral characterization of the chemogenetic model. D0.01 tissue was collected 30 minutes following CNO administration, a window designed to capture the immediate transcriptional response to parabrachial activation. This timepoint should reveal induction of immediate early genes (IEGs) such as *Fos*, *Nr4a1*, *Nr4a2*, and *Arc*, which serve as molecular markers of neuronal activation and initiate downstream transcriptional cascades involved in synaptic plasticity (Hochgerner et al., 2023). The IEG response is expected to identify which CeA populations are most immediately responsive to parabrachial input, potentially distinguishing direct postsynaptic targets from neurons engaged through polysynaptic or neuromodulatory mechanisms. However, the 30-minute window also captures early stress-responsive programs that may reflect nonspecific arousal rather than circuit-specific plasticity. To isolate activation-specific effects, both timepoints include mCherry-expressing control animals that receive identical CNO injections but lack hM3Dq expression; comparing hM3Dq

versus mCherry animals at D0 distinguishes transcriptional responses attributable to *Calca* neuron activation from those induced by injection, handling, or arousal alone.

D3 was selected to capture early consolidation processes following the acute response. Importantly, this timepoint ensures complete clearance of CNO and its metabolites: CNO plasma levels peak within 30 minutes of administration and fall to near-undetectable levels within 2-6 hours in rodents (Guettier et al., 2009; Manvich et al., 2018), meaning that any transcriptomic changes observed at D3 cannot reflect ongoing chemogenetic activation but must instead represent sustained or consolidation-phase alterations in gene expression. This timepoint falls within the window of hind-paw allodynia (Condon et al., 2024) and synaptic potentiation at PBN→CeA synapses described by Kissiwaa and Bagley (2018). who demonstrated that brief nociceptive stimulation induces potentiation peaking at 1–3 days post-stimulus (Kissiwaa & Bagley, 2018). Critically, D3 also falls within the transient period of calcium-permeable AMPA receptor incorporation at these synapses, a metaplastic state that creates vulnerability to cumulative sensitization if additional nociceptive input occurs (Kissiwaa & Bagley, 2018). By D3, immediate early gene expression should have largely returned to baseline, allowing identification of sustained transcriptional changes that may reflect consolidation of the plastic state rather than acute activation. The Kiritoshi et al. (2024) finding that acute and chronic neuropathic pain engage different cellular substrates, with CRH neurons showing hyperexcitability acutely but non-CRH populations predominating chronically, predicts that D0.01 and D3 may reveal distinct populations or gene programs, though their study examined longer timescales (1 week vs. 4 weeks) than the present design. The present analysis focuses on D0.01 and D3 timepoints to characterize the acute response and consolidation phase, with

particular attention to whether the cellular substrates of transcriptional activation shift across this interval.

The experimental design incorporates bilateral CeA collection following unilateral (right hemisphere) stimulation of parabrachial *Calca* neurons. This asymmetric design serves multiple analytical purposes. Parabrachial projections to CeA are primarily ipsilateral, though a minor contralateral component exists (Sah et al., 2003). Unilateral stimulation therefore produces asymmetric input to the two hemispheres, with the right (ipsilateral) CeA receiving strong direct monosynaptic drive while the left (contralateral) CeA receives weaker or indirect input. Collecting both hemispheres allows the left CeA to serve as a within-animal control, enabling hemisphere-stratified analyses that can distinguish treatment-specific effects from baseline inter-animal variability. This design also permits delta-delta analyses that separate stimulation-induced changes from any pre-existing hemispheric asymmetries in gene expression or cell type composition.

The hemisphere comparison is additionally motivated by evidence of lateralized pain processing in the CeA. As reviewed earlier, Allen et al. (2023) demonstrated that optogenetic activation of parabrachial *Calca* terminals in the right versus left CeA produces opposing effects on visceral pain sensitivity, with right-sided activation promoting hyperalgesia and left-sided activation producing antihyperalgesia (Allen et al., 2021, 2023). The present design provides an opportunity to examine whether transcriptomic responses differ between ipsilateral and contralateral CeA, which could reveal molecular correlates of lateralized pain processing if such asymmetries exist at the gene expression level.

Based on the literature reviewed above, several predictions can be articulated. First, we predict that D0.01 will show IEG enrichment concentrated in *Calcrl*-expressing populations,

which represent direct postsynaptic targets of parabrachial $CGRP^{+}$ terminals and occupy the capsular CeA territory most densely innervated by parabrachial afferents (S. Han et al., 2015; Palmiter, 2018; Wang et al., 2023). Second, we predict that D3 will reveal sustained transcriptional changes in partially overlapping but potentially distinct populations, possibly including *Prkcd* neurons, which show increased excitability in chronic pain states and may undergo transcriptional reprogramming during consolidation (Kiritoshi et al., 2024; Wilson et al., 2019). Third, we predict that treatment effects will be stronger in the right (ipsilateral) hemisphere than the left, reflecting the predominantly ipsilateral organization of parabrachial projections. Fourth, given the demonstrated hemispheric lateralization of CeA pain processing, we predict that some genes or pathways may show opposite regulation between hemispheres.

These predictions are necessarily tentative given the exploratory nature of single-cell transcriptomics. The molecular diversity revealed by recent CeA atlases, with functionally defined populations like "*Sst* neurons" or "*Prkcd* neurons" fragmenting into multiple transcriptionally distinct subtypes, means that responses may not map cleanly onto prior functional categories. The IEG response may be sparse and distributed across multiple populations rather than concentrated in a single cell type, as observed during fear learning (Hochgerner et al., 2023). Sustained changes at D3 may involve genes and pathways not previously implicated in CeA plasticity. The present study is therefore designed to both test specific hypotheses derived from prior circuit-level work and to generate new hypotheses about molecular mechanisms that can be pursued in subsequent functional studies.

This study addresses a significant gap in understanding the molecular programs through which parabrachial nociceptive input transforms CeA circuit function. By resolving transcriptomic responses at single-cell resolution across the acute-to-consolidation transition, the

findings aim to elucidate which specific CeA populations are engaged by *Calca*^{PBN} activation and how their gene expression programs evolve over the first three days after stimulation. This information is essential for understanding which cell types and molecular pathways represent viable therapeutic targets for interrupting the transition from acute to chronic pain. The study will also include a D14 time-point when the pain phenotype has resolved, but the sequencing data were not yet available for the analysis described here. The cross-species conservation of CeA cell types and neuropeptide systems suggests that findings from analyses like this one will have relevance for understanding the neural substrates of human nociplastic pain.

II. Methodology

Experimental Design and Sample Collection

Central amygdala (CeA) tissue was collected from *Calca*^{Cre} mice expressing either hM3Dq-mCherry or mCherry only in parabrachial nucleus (PBN) *Calca* neurons. All mice were prescreened by giving them CNO and measuring tactile sensitivity using the von Frey assay. Several weeks later the mice were used for this experiment. The analysis design comprised a 2×2×2×2 factorial structure: two timepoints, D0.01, 30 minutes post-CNO injection for acute transcriptional response; D3, 3 days post-injection for consolidation-phase changes), two treatment conditions (hM3Dq-expressing versus control), two hemispheres (left and right CeA), and two biological replicates per condition, yielding 16 independent samples (Table 1). Viral injection and chemogenetic activation were performed unilaterally in the right hemisphere of all animals, allowing the left hemisphere to serve as an internal control for baseline asymmetries while expecting the most pronounced differential transcription in the right (ipsilateral) CeA samples.

Table 1. Experimental Design and Sample Identification

*Sample ID**	Timepoint	Treatment	Hemisphere	Replicate	hM3dq Activity
D0.01-1 clCEA	D0.01	Control	Left	1	—
D0.01-1 crCEA	D0.01	Control	Right	1	—
D0.01-2 clCEA	D0.01	Control	Left	2	—
D0.01-2 crCEA	D0.01	Control	Right	2	—
D0.01-1_hlCEA	D0.01	hM3Dq	Left	1	Contralateral
D0.01-1 hrCEA	D0.01	hM3Dq	Right	1	Ipsilateral
D0.01-2 hlCEA	D0.01	hM3Dq	Left	2	Contralateral
D0.01-2 hrCEA	D0.01	hM3Dq	Right	2	Ipsilateral
C1 BC001 clCEA	D3	Control	Left	1	—
C1_BC002_crCEA	D3	Control	Right	1	—
C2 BC003 clCEA	D3	Control	Left	2	—
C2 BC004 crCEA	D3	Control	Right	2	—
H1 BC001 hlCEA	D3	hM3Dq	Left	1	Contralateral
H1 BC002 hrCEA	D3	hM3Dq	Right	1	Ipsilateral
H2_BC003_hlCEA	D3	hM3Dq	Left	2	Contralateral
H2_BC004_hrCEA	D3	hM3Dq	Right	2	Ipsilateral

Note: Sample naming convention: For D0.01 samples, format is D0.01-[replicate]_[treatment][hemisphere]CEA where c=control, h=hM3Dq, l=left, r=right. For D3 samples, format is [Treatment][Replicate]_BC00[X]_[treatment][hemisphere]CEA.

Single-Cell RNA Sequencing

Prior to my analysis, single-cell suspensions were prepared from paraformaldehyde-fixed, microdissected CeA tissue and processed using the 10X Genomics Chromium Flex protocol. D0.01 samples were processed as singleplexed reactions, while D3 samples were multiplexed. Raw sequencing data were aligned to the mouse reference genome (mm10) and processed through the Cell Ranger pipeline (10X Genomics) to generate filtered, feature-barcode matrices in H5 format.

Quality Control and Cell Filtering

Initial quality control was performed using Seurat v5 (Hao et al., 2024). Cells were retained if they met the following criteria: minimum of 250 detected genes, at least 500 unique molecular identifiers (UMIs), less than 20% mitochondrial gene content, and a transcriptional complexity score ($\log_{10}$GenesPerUMI) of at least 0.75. Adaptive upper thresholds for gene count and UMI

count were calculated per sample using the 98th percentile to account for sample-to-sample variation in sequencing depth. Potential doublets were identified and removed using scDblFinder (Germain et al., 2022).

Reference-Based Cell Type Validation

To ensure accurate anatomical assignment and restrict analysis to GABAergic CeA neurons, quality-filtered cells were submitted to the Allen Institute MapMyCells tool for hierarchical cell type classification against the Allen Brain Cell Atlas whole-mouse-brain reference (Yao et al., 2023). Cells were retained if they received GABAergic neuron classification at the class level with confidence scores ≥0.5. This validation step served both to confirm the GABAergic identity of retained cells and to identify any samples with potential tissue contamination from adjacent brain regions based on regional classification patterns. Cell barcodes passing MapMyCells validation were extracted and used to filter the corresponding Seurat objects.

Normalization

Gene expression data were normalized using SCTransform v2 with the glmGamPoi method for efficient parameter estimation (Choudhary & Satija, 2022). Both timepoints were processed using the 10X Genomics Flex protocol for fixed tissue, with D0.01 samples run as singleplexed reactions and D3 samples multiplexed, resulting in substantially lower sequencing depth in D3 samples (median UMI per cell: D3 ~3,700 vs D0.01 ~14,700; approximately 4-fold difference). SCTransform addresses this technical batch effect by modeling sequencing depth as an offset in the negative binomial regression, effectively removing depth-dependent variation without explicit regression. Mitochondrial gene percentage was regressed during normalization to remove remaining technical variation associated with cell stress or damage. Each sample was normalized independently with 5,000 initial variable features identified per sample, with the full

transcriptome retained for downstream differential expression analysis. Later, RPCA-based integration further mitigated depth-related batch effects across timepoints.

Multi-Sample Integration

Batch effects arising from sample-to-sample technical variation and the sequencing depth difference between timepoints were corrected using reciprocal principal component analysis (RPCA) integration within the SCTransform framework. Integration parameters were optimized through systematic parameter sweeps testing combinations of feature counts (2,000–5,000), principal component dimensions (1:25–1:45), UMAP neighbor and distance parameters, and anchor identification strategies. Final parameters were selected based on biological cluster resolution, appropriate mixing of technical replicates, and separation of biologically distinct populations.

The integration workflow proceeded as follows: 4,000 curated integration features were selected using SelectIntegrationFeatures, SCT models were prepared using PrepSCTIntegration, PCA was computed independently for each sample (50 components), integration anchors were identified using FindIntegrationAnchors with RPCA reduction across 35 dimensions (k.anchor = 5, k.filter = 200, k.score = 30, max.features = 200), and data were integrated using IntegrateData with SCT normalization (k.weight = 60, sd.weight = 1.2, eps = 0.1).

Clustering and Dimensional Reduction

Uniform Manifold Approximation and Projection (UMAP) was performed on the integrated data using 35 dimensions, 30 nearest neighbors, and minimum distance of 0.3. Graph-based clustering was performed using the Louvain algorithm following shared nearest neighbor (SNN) graph construction (k = 50 neighbors, 35 dimensions). Multiple clustering resolutions were evaluated (0.4, 0.6, 0.8, 1.0, 1.2); resolution 0.8 was selected based on balance between granularity and

biological interpretability, yielding sufficient resolution to distinguish known CeA subtypes while avoiding over-fragmentation.

Iterative Cluster Quality Control

Cluster quality was evaluated through multiple iterative passes to identify and remove contaminating non-CeA populations. Each cluster was assessed for GABAergic neuronal identity by requiring expression of at least two of three canonical markers (*Gad1, Gad2, Slc32a1*) above a normalized expression threshold of 0.3. CeA subtype identity was verified by requiring expression of established molecular markers from either Class 1 (amygdalostriatal transition, *Ppp1r1b*$^{+}$) or Class 2 (core CeA, *Nefm*$^{+}$) populations as defined by the Sternson atlas (Wang et al., 2023).

Clusters were flagged for removal if they exhibited: glutamatergic marker expression (*Slc17a6, Slc17a7*), non-neuronal signatures including astrocyte (*Gfap, Aqp4*), oligodendrocyte (*Mbp, Plp1, Mog*), or microglial (*P2ry12, Tmem119*) markers, or technical quality concerns including elevated doublet scores from scDblFinder, extreme sample bias (>80% of cells from a single sample), or anomalously small cluster size (<0.5% of total cells). Following iterative quality control, remaining clusters were renumbered consecutively.

Cell Type Annotation

Clusters were annotated based on expression of established CeA molecular markers, guided by the classification framework of Wang et al. (2023). Marker genes for each cluster were identified using FindAllMarkers on the SCT assay following PrepSCTFindMarkers preparation to enable proper comparison across samples with different sequencing depths. Markers were required to be expressed in at least 25% of cells within the cluster with a $\log_2$ fold-change threshold of 0.25 and adjusted p-value < 0.05 after Benjamini-Hochberg correction. Cluster identities were assigned

based on the top differentially expressed markers for each cluster, cross-referenced with the Wang et al. scRNA-seq clusters (seq-c1 through seq-c11) and EASI-FISH molecular clusters (MC-1 through MC-21). Clusters were named using their most distinguishing highly expressed markers organized by neuroanatomical subdivision: CeL populations (*Prkcd*/*Cartpt*, *Sst*/*Tac2*/*Vipr2*, *Sst*/*Pdyn*, *Crh*), CeC populations (*Calcrl*/*Cyp26b1*, *Prkcd*/*Calcrl*), and CeM output neurons (*Npy*, *Vdr*/*Nts*, *Gal*/*Gpx3*). Amygdalostriatal transition (AST) populations expressing D1-MSN markers (*Tac1*/*Drd1*/*Ppp1r1b*) or D2-MSN markers (*Drd2*/*Scn4b*/*Penk*) and intercalated cells (ITC) expressing *Foxp2*/*Tac2* were retained with explicit labels distinguishing them from core CeA neurons. Clusters exhibiting non-neuronal signatures (astrocyte, oligodendrocyte, endothelial, choroid plexus markers), glutamatergic markers (*Slc17a6*, *Slc17a7*), or cholinergic contamination (*Lhx8*) were excluded from downstream analysis.

Differential Expression Analysis

Differential expression analysis was performed using the SCT assay, which retains the full transcriptome rather than the reduced integration feature set. SCT models were prepared using PrepSCTFindMarkers to enable proper comparison across samples with different sequencing depths.

Given the unilateral nature of chemogenetic stimulation, differential expression was analyzed within the ipsilateral (right) hemisphere only, comparing hM3Dq-treated versus control samples. This approach focuses on the hemisphere receiving direct parabrachial input while avoiding potential confounds from baseline hemispheric asymmetries. For each cluster at each timepoint, the Wilcoxon rank-sum test was applied using Seurat's FindMarkers function, with multiple testing correction using the Benjamini-Hochberg procedure (FDR < 0.05). Genes were

required to be detected in at least 10% of cells in either comparison group (min.pct = 0.1) with no log fold-change threshold imposed to enable detection of small but reproducible effects.

To facilitate biological interpretation, significant DEGs were annotated into functional categories based on curated gene lists: canonical immediate early genes (*Arc, Bdnf, Btg2, Fos, Fosl2, Homer1, Npas4, Nr4a1, Jun, Junb, Jund, Egr1, Egr2, and Egr3*) transcription factors, G-protein-coupled receptors (including serotonin, GABA-B, opioid, and neuropeptide receptors), ion channels (GABA-A receptor subunits, AMPA/NMDA receptor subunits, voltage-gated potassium and calcium channels), neuropeptide precursors (*Penk*, *Pdyn*, *Sst*, *Crh*, *Tac1*, *Tac2*, *Npy*, etc.), and synaptic plasticity-related genes (*Camk2a*, *Camk2b*, *Shank1*, *Shank3*, *Homer1*, *Homer2*, *Bdnf*, *Mapk14*, etc.). This functional annotation enabled targeted analysis of biologically relevant gene classes as specified in the experimental aims.

Composition Analysis

Cell-type composition changes were assessed using the propeller function from the speckle package which implements a moderated statistical framework appropriate for compositional data derived from single-cell experiments (Phipson et al., 2022). Cell-level cluster assignments, sample identities, and treatment group memberships were provided as input vectors. Composition was compared between hM3Dq and control conditions separately at each timepoint to assess both acute perturbations and potential homeostatic compensation at the consolidation phase.

Immediate Early Gene Analysis

Acute neuronal activation was quantified using a 14-gene immediate early gene panel adapted from Hochgerner et al. (2023) with additional Jun and Egr family members: *Arc*, *Bdnf*, *Btg2*, *Fos*, *Fosl2*, *Homer1*, *Npas4*, *Nr4a1*, *Jun*, *Junb*, *Jund*, *Egr1*, *Egr2*, and *Egr3*. *Fosb* was excluded

from module scoring due to its longer accumulation kinetics but was tracked separately for consolidation timepoint analyses. IEG module scores were calculated per cell using Seurat's AddModuleScore function.

To account for the unilateral stimulation design, three comparison frameworks were applied at each timepoint: (1) pooled hM3Dq versus control across all hemispheres, using linear mixed effects models with treatment as fixed effect and animal as random effect; (2) within hM3Dq animals comparing ipsilateral (right) versus contralateral (left) hemispheres using Wilcoxon rank-sum tests; and (3) ipsilateral hemisphere only comparing hM3Dq-treated versus control animals using Wilcoxon rank-sum tests. P-values were corrected for multiple comparisons using the Benjamini-Hochberg procedure.

To characterize the transient IEG-high state (cluster C21), cells were subclustered on non-IEG variable features and their putative cell type origins were inferred by correlating each cell's non-IEG expression profile with mean expression profiles of the other clusters using Pearson correlation.

Gene Ontology and Pathway Enrichment

Gene Ontology (GO) enrichment analysis was performed on DEG sets from each cluster-timepoint combination using clusterProfiler (Yu et al., 2012) with the org.Mm.eg.db annotation database. Gene symbols were converted to Entrez IDs, and enrichment was tested against the Biological Process (BP) ontology using enrichGO with a background of all expressed genes. KEGG pathway enrichment was performed in parallel using enrichKEGG. Significance thresholds were set at $q < 0.05$ after Benjamini-Hochberg correction, with a minimum gene set size of 10 and maximum of 500. To assess temporal dynamics, GO terms were classified as D0.01-specific (significant only at D0.01), D3-specific (significant only at D3), or sustained

(significant at both timepoints). Pain- and plasticity-relevant terms were identified by keyword matching against term descriptions and curated manually for biological relevance.

Statistical Analysis

All statistical analyses were performed in R (v4.3). Multiple comparison correction using the Benjamini-Hochberg procedure was applied separately within each analysis framework as described below.

Cluster marker identification: Cluster-defining genes were identified using Seurat's FindAllMarkers function with the Wilcoxon rank-sum test. Genes were required to be expressed in at least 25% of cells in the target cluster (min.pct = 0.25) with a minimum log2 fold-change of 0.5. P-values were adjusted across all gene-cluster comparisons using the Benjamini-Hochberg procedure, with significance defined as adjusted $p < 0.05$.

Differential expression analysis: Treatment effects within cell populations were assessed using Seurat's FindMarkers function with the Wilcoxon rank-sum test. To enable detection of small but reproducible expression changes, genes were required to be detected in at least 10% of cells in either comparison group (min.pct = 0.1) with no log fold-change threshold. P-values were adjusted across all genes tested within each comparison using Benjamini-Hochberg correction.

IEG module score analysis: Three statistical frameworks were applied to account for the unilateral stimulation design. Pooled comparisons used linear mixed effects models with treatment as fixed effect and animal as random effect. Within-animal and hemisphere-matched comparisons used Wilcoxon rank-sum tests. For each framework, p-values were corrected across all clusters tested using the Benjamini-Hochberg procedure. Effect sizes represent the difference in mean module scores between groups.

Composition analysis: Cell type proportion changes were assessed using the propeller function from the speckle package (Phipson et al., 2022), which implements empirical Bayes moderation of cell type proportions and internal false discovery rate control.

C21 origin analysis: Cell type origins of the IEG-high cluster were inferred using Pearson correlation of expression profiles (excluding IEG genes) between C21 cells and main cluster centroids. This analysis was descriptive; no formal hypothesis testing was performed. Significance thresholds were set at adjusted $p < 0.05$ for all hypothesis tests.

Software Availability

Analyses were performed using R (v4.3) with the following packages: Seurat v5 for single-cell analysis and visualization, SCTransform v2 for normalization with regularized negative binomial regression, RPCA for batch correction within the Seurat integration framework, lme4 for linear mixed effects models, scDblFinder for doublet detection, speckle for compositional analysis using the propeller method, clusterProfiler for Gene Ontology enrichment, and ggplot2 for visualization. Custom R functions were developed for variable feature curation, cluster quality evaluation, and hemisphere-stratified differential expression analysis. Claude (Anthropic) was used to assist with learning R programming concepts and debugging code during analysis development.

III. Results and Discussion

A Molecularly Resolved Atlas of CeA GABAergic Neurons

To identify which CeA populations respond to parabrachial nociceptive input, we first needed to establish a comprehensive molecular taxonomy of the region. Following quality control filtering and validation of GABAergic identity through the Allen Institute MapMyCells pipeline, we retained 19,544 neurons that resolved into 21 transcriptionally distinct clusters (Fig. 1). This included 13 core CeA populations (C1-C13) spanning the lateral, capsular, and medial subdivisions, 5 amygdalostriatal transition zone populations (C14-C18), 1 intercalated cell cluster (C19), and 2 activity-state clusters (C20: Activity_low; C21: IEG_high). The activity-state clusters represent transient transcriptional states rather than stable cell types: C21 captures neurons during peak immediate early gene expression regardless of their underlying identity, while C20 contains neurons with unusually low expression of activity-regulated transcripts. These clusters emerged from the unsupervised clustering and were retained to track activation dynamics across conditions.

Integration across experimental conditions was successful: cells from both timepoints (D0.01, D3), treatment groups (hM3Dq, control), and hemispheres intermixed across all clusters without systematic batch effects (Fig. 2). Cell type proportions were consistent across the 16 samples (Fig. 3), and cell recovery was balanced between conditions (Fig. 4; D0.01: 10,740 cells; D3: 8,804 cells). This experimental balance enables robust statistical comparisons between treatment groups within each timepoint.

Our clustering recapitulated the molecular organization described by Wang et al. (2023), who defined 13 CeA populations using scRNA-seq of 1,393 neurons (Fig. 5). Nine of their clusters mapped clearly to populations in our dataset. The larger sample size in our study

provided additional resolution for populations relevant to pain processing: Wang et al. reported that *Calcrl* was distributed across their seq-c6 and seq-c8 clusters. We resolved this into three distinct populations: C8 (CeC_*Calcrl*; 2,874 cells) expressing *Calcrl* with capsular markers; C9 (CeC/CeL_*Prkcd-Calcrl*; 1,116 cells), a transitional population co-expressing *Calcrl* and *Prkcd*; and C10 (CeC_*Npy2r*; 607 cells), distinguished by *Npy2r* expression. This heterogeneity within CGRP-responsive populations proved important for understanding the temporal dynamics of parabrachial-driven activation.

Acute Parabrachial Activation Engages Specific CeA Subpopulations

Chemogenetic activation of parabrachial *Calca* neurons produced a robust but selective transcriptional response in the CeA at D0.01 (30 minutes post-CNO) compared to the control mice that only had a reporter gene but also received CNO. Because viral injection and thus stimulation was unilateral (right PBN), we employed hemisphere-stratified analysis, comparing hM3Dq versus control animals within the ipsilateral (right) hemisphere to isolate treatment effects from any baseline lateralization.

Four clusters showed significant IEG elevation at D0.01 (FDR < 0.05; Fig. 6). C9 (CeC/CeL_*Prkcd-Calcrl*) showed the strongest response among core CeA populations (effect size = 0.073, FDR = 0.013), followed by two AST populations: C18 (effect = 0.095, FDR = 0.020) and C16 (effect = 0.063, FDR = 0.033). C21 (IEG_high) showed strong elevation (effect = 0.26, FDR = 0.014), as expected given this cluster is defined by high activity gene expression. The identity of the most responsive core CeA population is notable. C9 is a transitional population co-expressing both *Prkcd* and *Calcrl*. Neither the "pure" *Prkcd* population (C1; effect = 0.028, FDR = 0.25) nor the largest *Calcrl*-expressing population (C8; effect = 0.003, FDR = 0.99) reached significance. This suggests that co-expression of both markers defines a

functionally distinct subpopulation positioned to respond to parabrachial CGRP input more strongly than populations expressing either marker alone.

PKCδ neurons in the CeL have been consistently implicated as direct postsynaptic targets of parabrachial CGRP terminals (Haubensak et al., 2010; Wilson et al., 2019). Our data refine this picture: within the broader PKCδ-expressing population, it is specifically the *Prkcd*/*Calcrl*-co-expressing subset (C9) that shows the most robust acute transcriptional response. C10 (CeC_*Npy2r*), which expresses *Calcrl* but not *Prkcd*, was not among the acutely responsive clusters (effect = 0.011, FDR = 0.99), further supporting the importance of PKCδ co-expression for acute CGRP responsiveness.

The activation of AST populations (C16 and C18, both D2-MSN subtypes) is notable given that parabrachial CGRP fibers do not directly innervate the AST (Wang et al., 2023), suggesting this response reflects polysynaptic propagation through CeA or other intra-amygdalar circuits. The AST has been implicated as a sensory interface during fear conditioning (LeDoux et al., 1988) and stress-enhanced fear conditioning increases neuronal activity specifically in the AST (Goto et al., 2022). Among the differentially expressed genes in C18, *Htr2c* (serotonin receptor 2c) showed marked upregulation (log2FC = 2.31). This is intriguing given that 5-HT2CR in the amygdala has been implicated in pain-related plasticity: knockdown of this receptor in the BLA reduces neuropathic pain behaviors and anxiety in rats (Ji et al., 2017), and 5-HT2CR-null mice show selectively enhanced affective responses to noxious stimuli (Bonasera et al., 2015). Whether AST activation and 5-HT2CR upregulation contribute to affective processing of parabrachial nociceptive signals warrants further investigation.

The IEG_high State Captures Neurons from Multiple Populations

The C21 cluster warrants special attention. Rather than representing a stable cell type, C21 captures neurons at peak IEG expression, a transient transcriptional state that neurons from multiple populations can enter. This phenomenon is well-established in amygdala transcriptomics: Hochgerner et al. (2023) demonstrated that during fear conditioning, only sparse subsets of neurons within each molecularly defined population upregulate IEGs, and that no single IEG reliably marks all activated neurons. They recommended using a consensus panel of activity-regulated genes, as we did, to identify these transient "IEG_high" states.

To determine which cell-types contribute to C21, we subclustered its 492 cells using non-IEG features and correlated each cell's expression profile with the centroids of the remaining clusters (Fig. 7, top panels). This analysis revealed four subclusters with distinct origins (Fig. 7, bottom panels). Subcluster 0 (n = 147 cells) derived primarily from C1 (CeL_*Prkcd*; 49%) and C9 (CeC/CeL_*Prkcd/Calcrl*; 46%), with best-match correlation to C9 (r = 0.91). Subcluster 1 (n = 134) showed mixed origins between C8 (CeC_*Calcrl*; 45%) and C10 (CeC_*Npy2r*; 43%). Subclusters 2 and 3 were dominated by C10-origin cells (50% and 33%, respectively).

The subclusters showed striking temporal segregation (Fig. 7, top right). Subclusters 0 and 3 were almost exclusively D0.01 cells (99.3% and 97.5% D0.01, respectively), while subcluster 2 was predominantly D3 cells (85.5% D3). This confirms that C21 is not a discrete neuronal subtype but a convergent activation state. The identity of neurons occupying this state shifts over time: *Prkcd*-expressing populations (C1, C9) dominate at D0.01, while *Npy2r*-expressing neurons (C10) increasingly contribute by D3 (Fig. 8).

This finding has methodological implications. Because C21 conflates multiple cell types in an activity-dependent manner, differential expression analysis within C21 would be

confounded by shifting cellular composition rather than reflecting transcriptional changes within a defined population. We therefore focus subsequent analyses on the core clusters (C1–C13), treating C21 as a readout of which populations are active rather than as an independent cell type.

Given ongoing work in the Palmiter lab examining hM3Dq-mediated stimulation of *Tacr1* (substance P receptor/NK1R) neurons in the CeA, we examined *Tacr1* expression and regulation across clusters. *Tacr1* showed broadly low baseline expression across CeA populations, with detectable expression in C11 (CeM_*Npy*), C4 (CeL_*Vipr2*), C2 (CeL_*Grik1*), and C6 (CeL_*Cbln4*). Notably, the strongest treatment-associated *Tacr1* upregulation occurred in C21 (IEG_high; log2FC = 1.18, p = 0.006), suggesting that *Tacr1*-expressing neurons are among those acutely activated by parabrachial stimulation. C11 (CeM_*Npy*) showed modest *Tacr1* elevation at both timepoints (D0.01 log2FC = 0.59; D3 log2FC = 0.84), though neither reached FDR significance. These findings indicate that while *Tacr1* neurons represent a minority of CeA cells, they are preferentially recruited during acute parabrachial activation, consistent with the known role of substance P signaling in nociceptive processing.

Temporal Dynamics: From Acute Alarm to Consolidation

The shift from *Prkcd*-dominant to *Npy2r*-dominant C21 composition between D0.01 and D3 suggests that different CeA populations are engaged at different phases following parabrachial activation. At D0.01, the IEG-high state is occupied primarily by neurons from C1 (26.9%) and C9 (21.7%), populations expressing *Prkcd* that receive direct CGRP input and drive behavioral responses to acute threat (Ciocchi et al., 2010; Haubensak et al., 2010). (By D3, C1 contribution dropped to 3.2% while C10 (CeC *Npy2r*) rose from 23.9% to 50.8% of C21 cells (Fig. 8).

The emergence of *Npy2r*-expressing neurons as the dominant contributor to residual activity at D3 is notable given what is known about NPY signaling in the amygdala. The Y2 receptor is

predominantly a presynaptic autoreceptor that inhibits neurotransmitter release, including NPY, GABA, and glutamate (Verma et al., 2015). In the CeA, NPY-expressing and Y2R-expressing neurons represent largely non-overlapping populations; Y2R-positive cells receive NPY input rather than providing it (Verma et al., 2015) . Functionally, Y2R signaling has been implicated in both anxiety-like behavior and the long-term suppression of conditioned fear (Tasan et al., 2016).

Importantly, this compositional shift occurred against a backdrop of normalizing IEG levels. By D3, no cell type showed significant IEG elevation when comparing hM3Dq-treated to control animals within the ipsilateral hemisphere (Fig. 9). The acute transcriptional burst is thus transient, consistent with the canonical role of IEGs as activity markers rather than sustained plasticity indicators. Yet C21 IEG activity persists at D3, now populated predominantly by C10-origin cells, with C1 (CeL_*Prkcd*) maintaining a reduced but notable presence. This suggests low-level but ongoing activity in *Npy2r*-expressing neurons, with potential contributions from PKCδ populations, a residual signal that may reflect consolidation processes rather than acute activation.

Whether the shift from *Prkcd* to *Npy2r* dominance represents adaptive plasticity (tuning of nociceptive thresholds, consolidation of threat memory) or the early stages of maladaptive sensitization cannot be determined from transcriptional data alone. Moreover, the C1 neurons that remain in the IEG-high state at D3, though reduced in proportion, may represent a subset with distinct consolidation-phase functions. Identifying the molecular programs active in C10, C1, and other populations that maintain C21 representation at D3 requires differential expression analysis beyond IEG markers.

Differential Gene Expression in Pain-Relevant Populations

To characterize the broader transcriptional programs engaged by parabrachial activation beyond IEG markers, we performed differential expression analysis comparing hM3Dq-treated versus control animals within each cluster at each timepoint. Using Wilcoxon rank-sum tests with Benjamini-Hochberg correction (FDR < 0.05), we identified 1,872 significant DEGs at D0.01 and 4,787 at D3 across all clusters (Fig. 10A). At D0.01, the clusters with the most DEGs were C14 (AST_D1-MSN; 224 genes), C8 (CeC_*Calcrl*; 196 genes), and C20 (Activity_low; 172 genes). By D3, this distribution shifted substantially: C2 (CeL_*Grik1*) showed the largest response with 1,291 DEGs, followed by C14 (596), C8 (583), and C1 (CeL_*Prkcd*; 529).

A striking asymmetry emerged in the direction of expression changes between timepoints. At D0.01, DEGs were roughly balanced between upregulation (910 genes) and downregulation (962 genes). By D3, this balance shifted dramatically: only 181 genes showed increased expression while 4,606 showed decreased expression, a 25-fold bias toward transcript suppression (Fig. 10B). This asymmetry was reflected in functional gene categories, particularly plasticity-associated genes: of 215 plasticity gene hits at D3, 165 (77%) were downregulated. Notably, key synaptic plasticity effectors showed exclusive downregulation across multiple clusters, including *Camk2a* and *Camk2b* (CaMKII subunits, detected in 11 and 14 clusters respectively), *Shank1* and *Shank3* (postsynaptic scaffolds), and *Dlg4* (PSD-95). Transcription factors also showed a downregulation bias (143 down vs 93 up), with *Foxo3* downregulated across six clusters. The temporal pattern of functional DEGs in pain-relevant clusters is summarized in Fig. 11C.

The sole exception to this downregulation pattern at D3 was neuropeptide precursor genes: *Penk* (proenkephalin) showed significant upregulation in C3 (CeL_*Crh*), C17

(AST_*Drd2*-MSN), and C19 (ITC_Foxp2/Tac2), while *Pdyn* (prodynorphin) was upregulated in C15 (AST_*Drd1*-MSN). This selective induction of opioid peptide precursors against a background of widespread transcriptional suppression suggests engagement of endogenous analgesic or stress-modulatory systems during the consolidation phase.

Acute Transcriptional Programs in Pain-Relevant Clusters

Focusing on the pain-relevant clusters identified by IEG analysis (C1, C5, C8, C9), we examined which specific genes drove the acute response at D0.01. C9 (CeC/CeL_*Prkcd/Calcrl*), the cluster showing strongest IEG elevation, had six canonical IEGs reach significance: *Egr1* (log2FC = 1.68), *Egr4* (log2FC = 1.77), *Arc* (log2FC = 2.62), *Junb* (log2FC = 0.69), *Jund* (log2FC = 0.91), and *Dusp1* (log2FC = 1.07) (Fig. 11A). The co-induction of *Egr1* and *Egr4* is notable: these zinc-finger transcription factors are rapidly induced by neuronal activity and regulate distinct downstream gene programs involved in synaptic plasticity. *Arc*, showing the largest fold-change, encodes activity-regulated cytoskeleton-associated protein with established roles in AMPA receptor trafficking and synaptic scaling—processes directly implicated in pain-related plasticity at PBN-CeA synapses (Kissiwaa & Bagley, 2018).

C8 (CeC_*Calcrl*), though not reaching significance for overall IEG elevation, showed acute upregulation of two activity-dependent transcription factors: *Atf2* (log2FC = 0.56) and *Mef2a* (log2FC = 0.53) (Fig. 11B). ATF2 is a CREB family member that can be activated by stress-activated protein kinases (p38, JNK), while MEF2A regulates activity-dependent synapse development. The upregulation of these transcription factors in a cluster defined by CGRP receptor expression is notable, though CGRP receptor signaling occurs primarily through cAMP-PKA rather than the calcium-dependent pathways that typically engage ATF2 and MEF2A, suggesting either crosstalk between signaling cascades or contributions from concurrent

glutamatergic input. C8 also showed acute upregulation of *Grik2* (log2FC = 0.44; encoding GluK2 kainate receptor subunit), upregulation of *Dusp6* (log2FC = 1.34; a MAPK phosphatase involved in ERK signaling termination), and downregulation of *Sstr5* (log2FC = −0.45; somatostatin receptor 5), suggesting early retuning of both glutamatergic signaling and peptidergic modulation.

C1 (CeL_*Prkcd*) showed a distinct acute signature characterized by upregulation of all three calmodulin genes, *Calm1* (log2FC = 0.27), *Calm2* (log2FC = 1.07), and *Calm3* (log2FC = 0.32), and downregulation of *Tac1* (log2FC = −1.37), encoding the substance P/neurokinin A precursor. The coordinated calmodulin upregulation indicates engagement of calcium-dependent signaling cascades, while *Tac1* downregulation may reflect feedback inhibition of tachykinin signaling following intense activation. C5 (CeL_*Sst/Pdyn*), by contrast, showed no significant functional category DEGs at D0.01 (Fig. 11C), consistent with somatostatin neurons being less directly engaged by acute parabrachial input than PKCδ-expressing populations.

Consolidation-Phase Transcriptional Remodeling

By D3, the transcriptional landscape had shifted dramatically. Total DEG counts in pain-relevant clusters expanded 3- to 5-fold: C1 from 120 to 529, C5 from 54 to 251, C8 from 196 to 583, and C9 from 80 to 309 (Fig. 12C). More striking than the quantity was the qualitative shift in gene categories and the overwhelming predominance of downregulation. Whereas D0.01 showed balanced expression changes with IEGs and transcription factors as prominent upregulated classes, D3 was characterized by broad suppression of ion channels, synaptic scaffolding components, and signaling molecules.

In C8 (CeC_*Calcrl*), the ion channel genes reaching significance at D3 were exclusively downregulated: *Gria4* (log2FC = −0.41; encoding AMPA receptor subunit GluA4) and *Gabra4*

(log2FC = −0.40; encoding GABA-A receptor α4 subunit) (Fig. 12A). The coordinated downregulation of both excitatory and inhibitory receptor subunits suggests active remodeling of synaptic receptor composition rather than simple scaling of transmission strength. The *Gria4* finding is particularly relevant given established evidence that pain-related plasticity at PBN-CeA synapses involves changes in AMPA receptor subunit composition, including transient incorporation of calcium-permeable (GluA2-lacking) receptors during the consolidation window (Kissiwaa & Bagley, 2018). Transcriptional downregulation of *Gria4* may reflect compensatory changes accompanying this functional subunit switch.

C8 also showed coordinated downregulation of three postsynaptic scaffolding genes: *Camk2b* (log2FC = -0.43), *Shank3* (log2FC = -0.32), and *Homer2* (log2FC = -0.59) (Fig. 12B). These proteins form the core structural framework of postsynaptic densities, linking glutamate receptors to intracellular signaling cascades and the actin cytoskeleton. Their coordinated downregulation at D3, occurring against a background of functional potentiation (Kissiwaa & Bagley, 2018), suggests active reorganization of postsynaptic architecture, potentially reflecting a transition from an unstable plastic state toward a consolidated new configuration.

C9 (CeC/CeL_*Prkcd/Calcrl*) showed a distinct pattern of ion channel downregulation at D3: *Kcnd2* (log2FC = −0.68; Kv4.2 A-type potassium channel), *Gabra1* (log2FC = −1.51; GABA-A receptor α1 subunit), and *Kcnk9* (log2FC = −0.78; TASK-3 two-pore potassium channel). Kv4.2 channels mediate transient outward currents that regulate dendritic excitability and back-propagating action potentials; their downregulation would be expected to increase dendritic integration of synaptic inputs. The large *Gabra1* decrease (the strongest fold-change among C9 ion channels) suggests substantial remodeling of GABAergic inhibition in this population. C1 (CeL_*Prkcd*) showed mixed AMPA receptor regulation: downregulation of

Gria3 (log2FC = −0.43) but upregulation of *Gria1* (log2FC = 0.36) and the R-type calcium channel *Cacna1e* (log2FC = 0.55), indicating subunit-specific remodeling rather than global scaling.

The synaptic organizer *Grid1* (encoding GluD1) showed significant downregulation at D3 in C2 (CeL_*Grik1*; log2FC = −0.53, FDR p = 0.002), with consistent downward trends in C5 (log2FC = −0.56), C8 (log2FC = −0.26), and C10 (log2FC = −0.35). GluD1 forms a trans-synaptic complex with presynaptic cerebellin-1 (*Cbln1*) and neurexin that maintains synaptic structure at PBN-CeA synapses (Gandhi et al., 2021). In inflammatory and neuropathic pain models, *Grid1* and *Cbln1* transcription are downregulated while AMPA receptor expression increases, and exogenous Cbln1 produces sustained reversal of mechanical hypersensitivity through restoration of this signaling complex (Gandhi et al., 2021). The *Grid1* downregulation observed here thus represents a molecular signature shared between chemogenetic parabrachial activation and persistent pain states.

However, the cell-type distribution differs from that reported in pain models. Gandhi et al. (2021) found GluD1 expression specifically on *Prkcd* neurons in the CeLC using immunohistochemistry, with minimal expression on somatostatin neurons. In our data, the strongest *Grid1* effect appeared in C2, a *Grik1*-expressing population distinct from the *Prkcd* clusters C1 and C9. This discrepancy may reflect differences between the experimental paradigms: inflammatory and neuropathic pain involve sustained peripheral input over days to weeks, engaging canonical nociceptive pathways, whereas acute chemogenetic activation produces a temporally compressed stimulus that may recruit broader CeA circuitry. The appearance of *Grid1* downregulation in C2 neurons, which were not identified in smaller reference datasets and may represent a novel CeA population, suggests that intense parabrachial

activation can engage synaptic remodeling programs beyond the classically defined pain-responsive *Prkcd* populations.

The transcription factor *Foxo3* showed particularly consistent downregulation across clusters at D3, reaching significance in C1 (log2FC = -0.85), C5 (log2FC = -1.92), C8 (log2FC = -0.84), C10 (log2FC = -0.96), C14 (log2FC = -1.06), and C18 (log2FC = -1.20). FOXO3 regulates cellular stress responses, autophagy, and apoptosis; its widespread suppression may reflect a shift from stress-responsive transcriptional states toward stable, activity-adapted programs. The acute-upregulated transcription factor *Atf2* showed the opposite trajectory: upregulated in C8 at D0.01, it was significantly downregulated in C10 at D3 (log2FC = -1.25), consistent with temporal handoff from immediate-response to consolidation-phase transcriptional regulators.

Temporal Separation of Acute and Consolidation Programs

A critical question for understanding pain-related plasticity is whether the consolidation-phase transcriptional program represents persistence or amplification of the acute response, versus engagement of fundamentally distinct molecular mechanisms. To address this, we examined the overlap between genes reaching significance at D0.01 versus D3 within each cluster (Fig. 13). The results revealed remarkably little overlap. In C8 (CeC_*Calcrl*), of 196 genes significant at D0.01 and 583 at D3, only 15 showed sustained differential expression at both timepoints (Fig. 13A). The remaining 181 D0.01 DEGs were acute-resolved (significant only at the early timepoint) while 568 D3 DEGs were consolidation-emergent (not detected acutely but appearing by the early consolidation phase). Among the acute-resolved genes were *Slc17a7* (vGluT1, upregulated acutely), *Dusp6* (MAPK phosphatase), and *C1ql3* (complement-related synapse organizer). Consolidation-emergent genes included *Eef2* (elongation factor 2, a translation factor

critical for protein synthesis), *Egr3* (a late-response transcription factor distinct from the acute *Egr1*/*Egr4* response), and the GABA-A receptor subunit *Gabra4*. The sustained genes included *Tspoap1* (TSPO-associated protein), *Syn2* (synapsin II), and *Basp1* (brain acid soluble protein 1).

C9 (CeC/CeL_*Prkcd/Calcrl*) showed even more striking temporal separation: of 80 D0.01 DEGs and 309 D3 DEGs, only a single gene (*Tspoap1*) reached significance at both timepoints (Fig. 13B). The acute-resolved genes included the IEGs *Arc* and *Egr4* that defined C9's acute response, as well as *Ptprb* (receptor-type tyrosine-protein phosphatase β) and *Cdkn1b* (p27 cell cycle inhibitor). These activation markers returned to baseline by D3 even as a much larger consolidation program emerged. The near-complete non-overlap (0.3% of combined DEGs) indicates that acute activation and early consolidation engage almost entirely distinct transcriptional programs in this population.

This minimal overlap has important implications for understanding pain-circuit plasticity. It indicates that acute activation and early consolidation involve largely distinct transcriptional programs rather than simple persistence or amplification of initial responses. The finding aligns with electrophysiological evidence that different cellular substrates contribute to acute versus chronic pain states. Kiritoshi et al. (2024) demonstrated that CRH neurons show hyperexcitability in acute neuropathic pain models while non-CRH populations predominate in the chronic phase. Our transcriptional data extend this framework by showing that even within a given cell type (e.g., C8 *Calcrl*$^{+}$ neurons), the genes engaged acutely are almost entirely distinct from those engaged during consolidation.

Pathway Enrichment Analysis

To understand the functional significance of these expression changes at the pathway level, we performed Gene Ontology (GO) enrichment analysis on the DEG sets from each cluster and

timepoint. Applying a stringent FDR threshold ($q < 0.05$), we identified 253 significantly enriched biological process terms across all conditions. The temporal distribution of these terms reinforced the pattern observed at the single-gene level: 221 terms (87%) were specific to D3, only 28 terms (11%) were specific to D0.01, and just 4 terms showed enrichment at both timepoints (Fig. 14A).

The four terms enriched at both timepoints: vesicle-mediated transport in synapse, inorganic ion homeostasis, intracellular cation homeostasis, and intracellular ion homeostasis, represent core synaptic and cellular maintenance functions that would be expected to accompany any substantial transcriptional perturbation. Their presence at both timepoints likely reflects the shared cellular context of neuronal activation rather than a specific plastic mechanism. D0.01-specific terms were predominantly metabolic and housekeeping processes: maintenance of location, maintenance of location in cell, carbohydrate biosynthetic process, and monosaccharide biosynthetic process. These likely reflect the immediate metabolic demands of acute neuronal activation rather than circuit-specific plasticity mechanisms. D3-specific terms, by contrast, were dominated by processes directly relevant to synaptic plasticity and circuit remodeling: neuron projection maintenance (enriched in C8 and C2), neurotransmitter transport (C8, C2), positive regulation of synaptic transmission (C1), regulation of neuronal synaptic plasticity (C8, C2), and cellular response to amyloid-beta (C8, C2). Several terms related to amyloid precursor protein (APP) processing appeared across multiple clusters (C1, C2, C3, C8), which is notable given APP's established roles in synaptic plasticity and trans-synaptic signaling. Interleukin-1 production and regulation of cytokine production were enriched specifically in C3 (CeL_*Crh*), suggesting neuroimmune pathway engagement in CRH-expressing neurons.

To specifically assess pain- and plasticity-related pathway engagement, we curated a subset of GO terms directly relevant to these processes and examined their distribution across CeA clusters and timepoints (Fig. 14B). Of the pain- or plasticity-related terms enriched in canonical CeA populations (C1-C13), the vast majority appeared exclusively at D3, indicating consolidation-specific pathway activation. Multiple clusters showed engagement: C1 (CeL_*Prkcd*) showed enrichment for behavioral response to pain, long-term synaptic potentiation, and synapse assembly; C8 (CeC_*Calcrl*) showed enrichment for regulation of dendritic spine maintenance, regulation of neuronal synaptic plasticity, vesicle-mediated transport in synapse, signal release from synapse, and negative regulation of long-term synaptic potentiation; and C2 (CeL_*Grik1*) showed enrichment for response to pain and synaptic vesicle exocytosis. The enrichment of negative regulation of LTP in C8 is particularly relevant: it suggests active engagement of homeostatic mechanisms that constrain runaway potentiation, consistent with the transcriptional downregulation of plasticity effectors observed at the single-gene level.

A Framework for Pain Circuit Consolidation

Integrating across levels of analysis, from IEG markers to individual DEGs to pathway enrichment, a coherent temporal framework emerges for CeA responses to parabrachial nociceptive input. The acute phase (D0.01, 30 minutes post-activation) is characterized by sparse but intense IEG induction in specific populations, particularly C9 (*Prkcd*/*Calcrl* co-expressing neurons) where *Arc*, *Egr1*, and *Egr4* showed 1.7- to 2.6-fold upregulation, with concurrent activation of calcium-dependent transcription factors (*Atf2*, *Mef2a* in C8) and calmodulin signaling (*Calm1*/*Calm2*/*Calm3* in C1). The consolidation phase (D3) shows resolution of IEG elevation but massive expansion of downstream programs, with a striking 25:1 bias toward

transcriptional suppression rather than induction. Ion channels, synaptic scaffolds (*Camk2a*/*Camk2b*, *Shank3*, *Homer2*), GPCRs, and the stress-responsive transcription factor *Foxo3* are broadly downregulated, while opioid peptide precursors *Penk* and *Pdyn* are selectively induced.

This framework aligns with and extends electrophysiological characterization of the PBN-CeA pathway. Kissiwaa and Bagley (2018) demonstrated that brief nociceptive stimulation induces synaptic potentiation at PBN-CeA synapses that peaks at 1-3 days, with the D3 timepoint falling within this maximal potentiation window. They further showed that this potentiation involves biphasic changes in AMPA receptor composition: transient incorporation of calcium-permeable receptors followed by return to GluA2-containing receptors, which creates a metaplastic vulnerability window (Kissiwaa & Bagley, 2018). Our transcriptional data provide a molecular substrate for these functional observations: the coordinated downregulation of *Gria3*, *Gria4*, *Gabra1*, *Gabra4*, and scaffolding proteins at D3 likely reflects the transcriptional correlates of receptor trafficking and postsynaptic reorganization underlying functional potentiation. The predominance of transcriptional suppression, paradoxical in the context of synaptic strengthening, may reflect homeostatic compensation that stabilizes the potentiated state, or alternatively, active refinement that prunes unnecessary components of an initially broad plastic response.

The near-complete temporal separation between D0.01 and D3 transcriptional programs (only 15 shared genes in C8, just 1 in C9) suggests that the acute-to-consolidation transition involves a fundamental switch in molecular mechanisms rather than simple persistence of initial responses. The acute program (IEGs, immediate transcription factors like *Atf2*) initiates plasticity; the consolidation program (receptor subunit regulation, scaffold reorganization, *Foxo3*

suppression) implements and stabilizes it. Disrupting either phase would be expected to have different consequences for the development of persistent pain states, a distinction with potential therapeutic implications.

Several limitations warrant acknowledgment. Our design captures only two timepoints, missing both the immediate-early phase (minutes) and later consolidation (weeks). The D0.01 timepoint, collected 30 minutes post-CNO, may conflate true immediate responses with early secondary cascades. The chemogenetic activation paradigm, while providing precise circuit control, may not fully recapitulate the transcriptional programs engaged by peripheral injury. And the pooled sample design, while enabling cost-effective multi-condition analysis, limits statistical power for detecting subtle effects. Despite these limitations, the convergence between our findings and those from injury-based models, particularly regarding the temporal dynamics of plasticity gene expression and the involvement of specific receptor families, supports the relevance of chemogenetic activation as a model system for studying pain circuit plasticity. Future directions include extending the temporal analysis to later timepoints (D14) to characterize the transition from early consolidation to resolution states, cell-type-specific manipulation of identified candidate genes (particularly *Foxo3*, *Camk2b*, and *Gria4*) to test their functional contributions to pain-related plasticity, and integration with proteomic and electrophysiological approaches to link transcriptional changes to functional synaptic modifications. The molecular taxonomy established here, particularly the identification of C8 and C9 as transcriptionally responsive populations with distinct temporal dynamics, provides a foundation for such investigations.

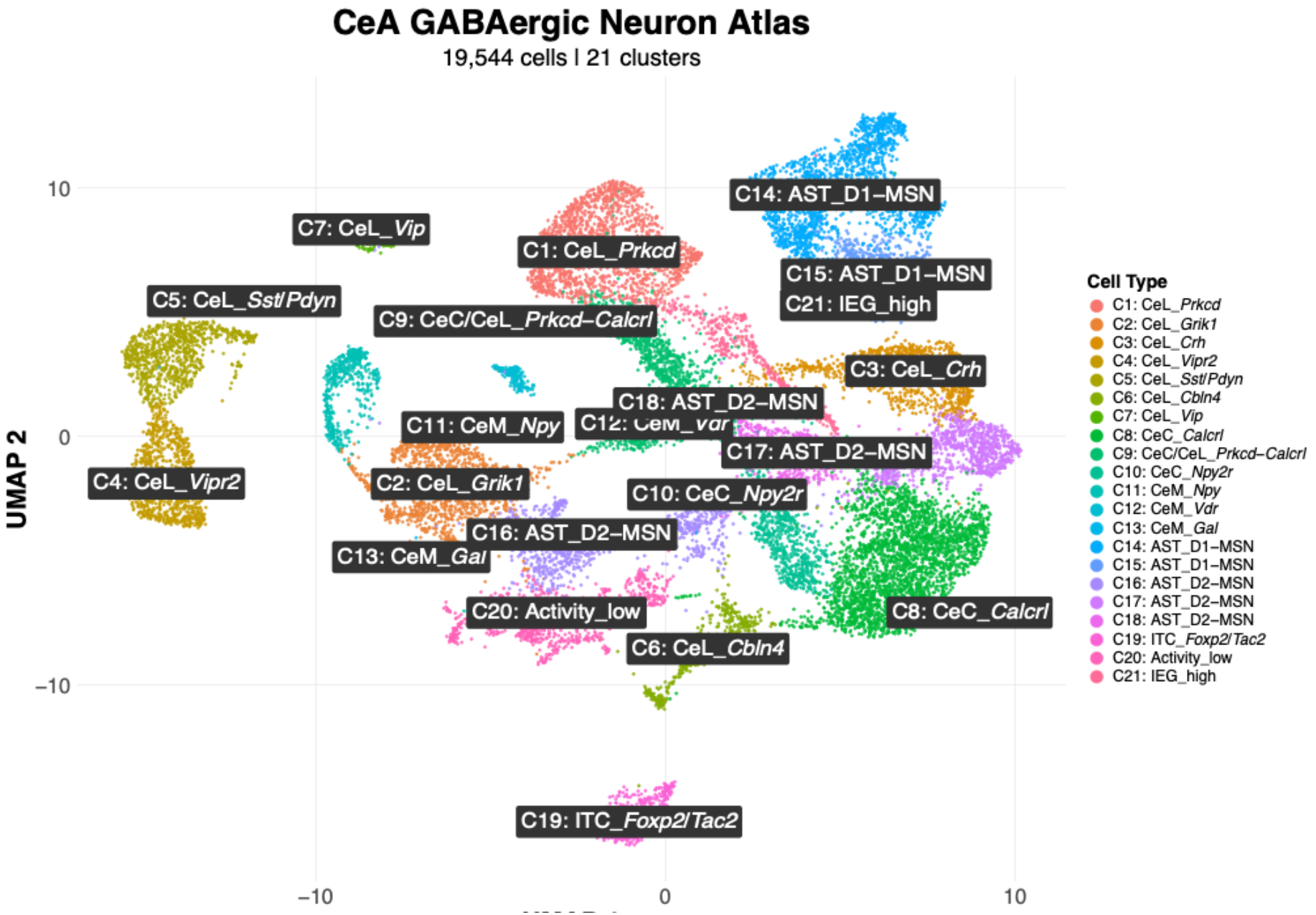

Figure 1. Single-cell transcriptomic atlas of CeA GABAergic neurons.

UMAP visualization of 19,544 GABAergic neurons from the central amygdala following quality control filtering and reference-based validation through the Allen Institute MapMyCells pipeline. Unsupervised clustering resolved 21 transcriptionally distinct populations, including 13 core CeA neuronal types (C1–C13), 5 amygdalostriatal transition zone populations (C14-C18), 1 intercalated cell cluster (C19), and 2 activity-state clusters (C20-C21). Cluster annotations reflect canonical marker gene expression, with defining markers indicated in parentheses. Colors are grouped by anatomical region: lateral CeA (CeL, warm colors), capsular CeA (CeC, greens), medial CeA (CeM, blues), amygdalostriatal transition zone (AST, purples), and intercalated cells (ITC, brown). Data represent pooled samples from D0.01 (30 min) and D3 (3 day) timepoints across control and hM3Dq treatment conditions.

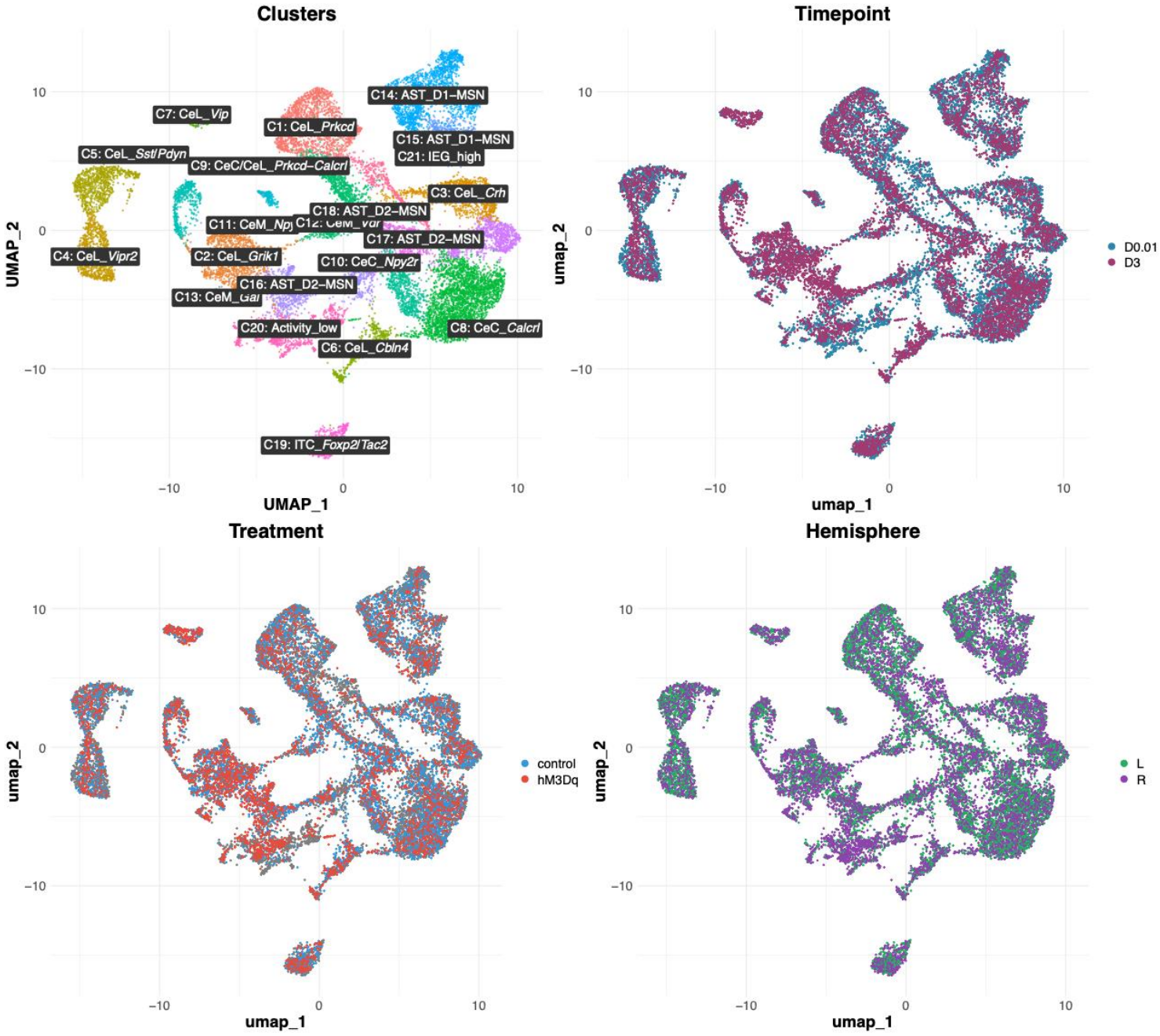

Figure 2. Distribution of cells across experimental conditions.

UMAP visualizations colored by timepoint (D0.01, blue; D3, red), treatment (control, gray; hM3Dq, red), and hemisphere (left/contralateral, green; right/ipsilateral, purple). Cells from all conditions intermix across clusters, indicating successful batch correction and absence of systematic technical artifacts. The balanced representation across conditions enables robust statistical comparisons between treatment groups and timepoints.

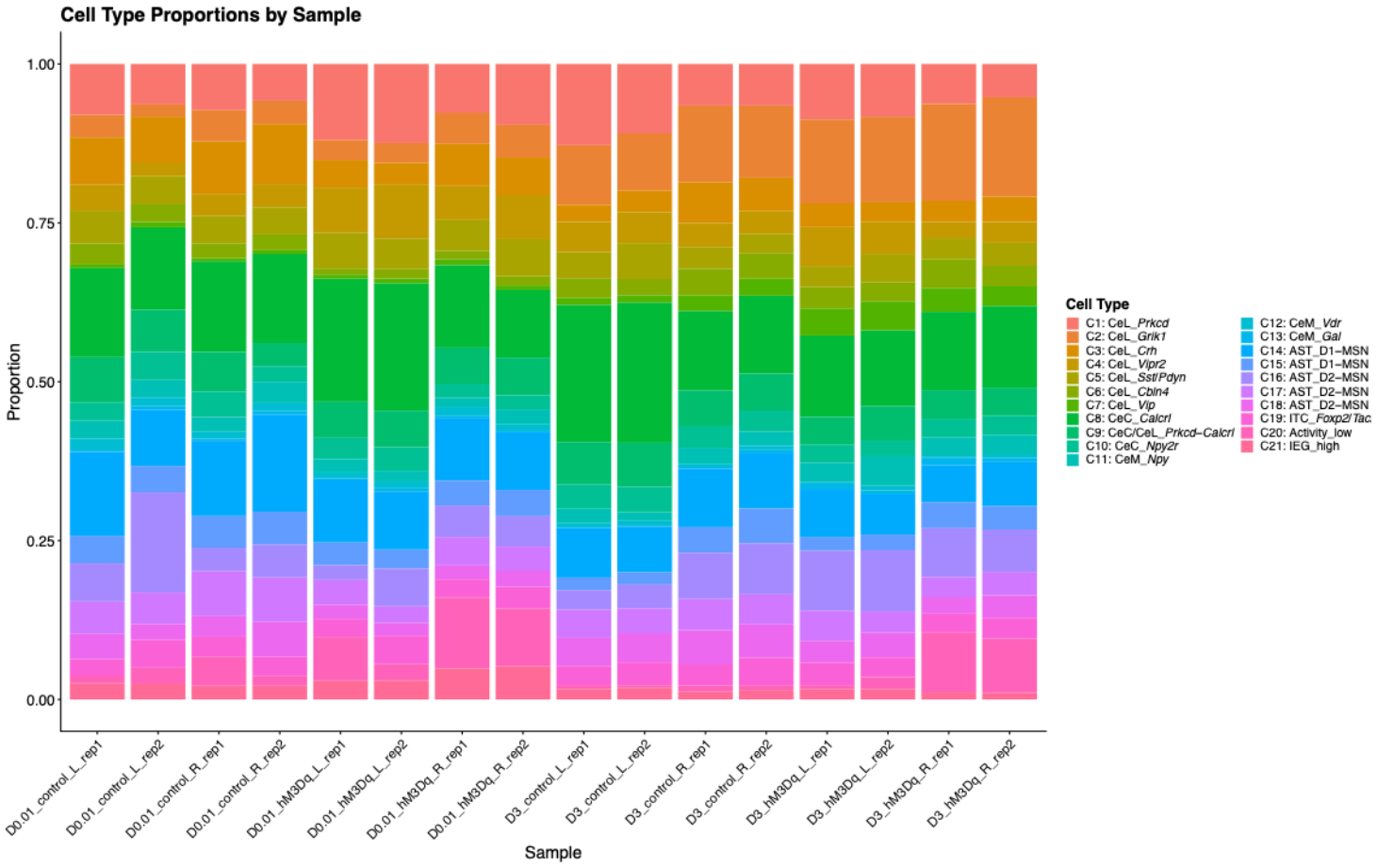

Figure 3. Cell type proportions across samples.
Stacked bar plot showing the proportional representation of each cluster across all 16 samples. Sample labels indicate timepoint (D0.01, D3), treatment (control, hM3Dq), hemisphere (L, R), and biological replicate. Consistent proportions across samples within conditions

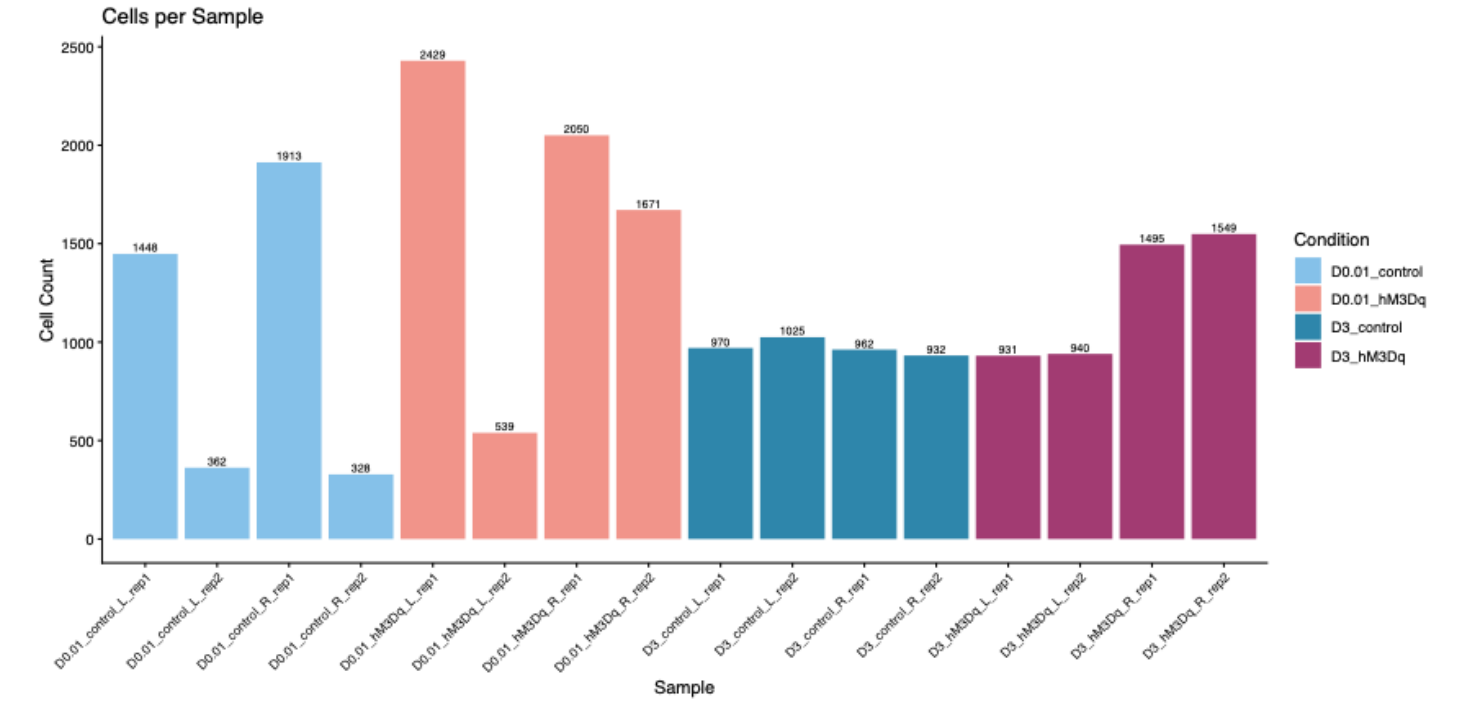

Figure 4. Cell recovery per sample.
Bar plot showing the number of cells recovered from each of the 16 samples following quality control filtering. Samples are labeled by timepoint (D0.01, D3), treatment condition (control, hM3Dq), hemisphere (L = left/contralateral, R = right/ipsilateral), and biological replicate. Cell recovery varied across samples, ranging from 328 to 2,429 cells per sample. D0.01 samples yielded 10,740 total cells; D3 samples yielded 8,804 total cells. Color indicates experimental condition.

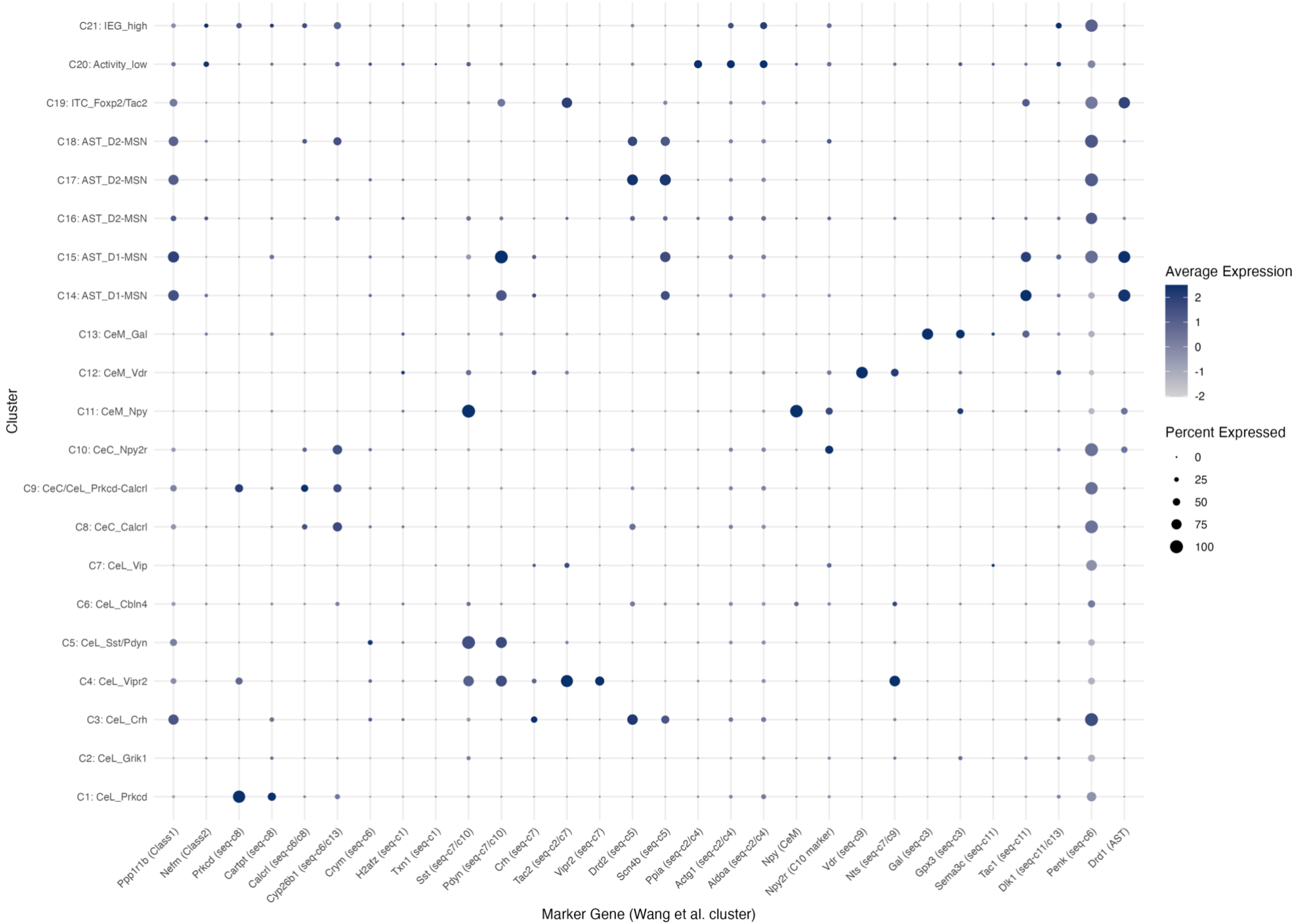

Figure 5. Comparison to established CeA molecular taxonomy.
Dot plot of marker genes defined by Wang et al. (2023) across the 21 identified clusters. Dot size indicates percentage of cells expressing each gene; color intensity reflects average expression level. Markers include class identity genes (*Ppp1r1b*, *Nefm*), *Prkcd* population markers (*Prkcd*, *Cartpt*), *Sst*/*Pdyn* markers (*Sst*, *Pdyn*, *Vipr2*, *Tac2*), CeM markers (*Npy*, *Vdr*, *Gal*), CGRP-responsive markers (*Calcrl*, *Npy2r*), and striatal markers for AST populations (*Drd1*, *Drd2*). Nine of 13 Wang et al. clusters showed clear correspondence to populations in our dataset.

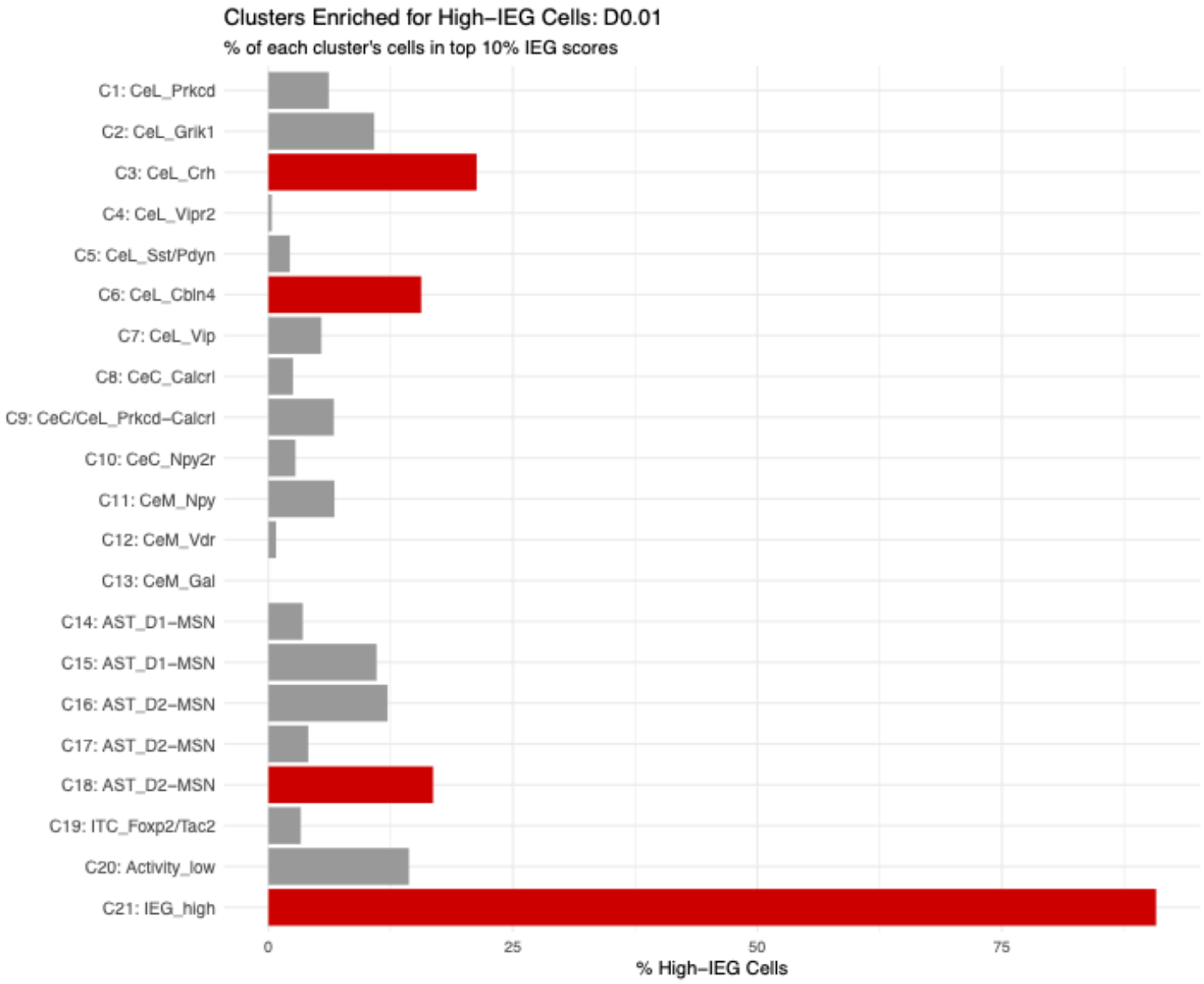

Figure 6. Acute IEG elevation at D0.01 by cell type.

Bar plot showing IEG composite score effect sizes for each of the 21 cell types at D0.01 (30 min post-stimulation), comparing ipsilateral (right) hemispheres between hM3Dq-treated and control animals. This hemisphere-matched

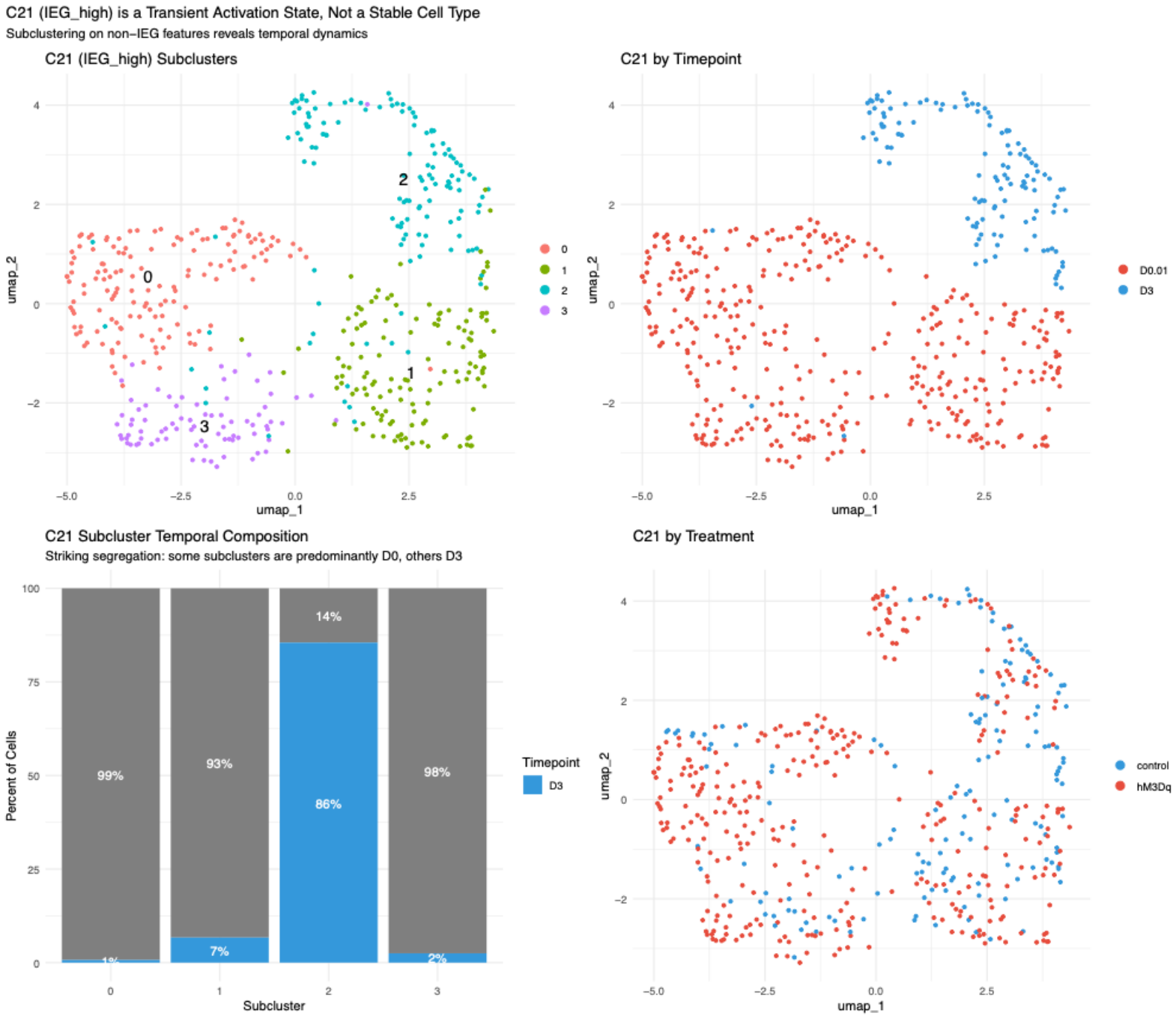

Figure 7. C21 (IEG_high) represents a transient activation state, not a stable cell type.

Subclustering of C21 cells on non-IEG features reveals that this population comprises neurons entering a shared high-activity transcriptional state with distinct temporal dynamics. (Top left) UMAP visualization of C21 cells colored by subcluster identity (0–3). (Top right) The same cells colored by timepoint show striking temporal segregation, with subclusters 0 and 1 predominantly containing D0.01 cells while subclusters 2 and 3 are enriched for D3 cells. (Bottom left) Stacked bar plot quantifying the temporal composition of each subcluster, confirming that subclusters 0-1 are >93% D0.01 while subclusters 2-3 are >86% D3. (Bottom right) UMAP colored by treatment shows that C21 cells derive from both control and hM3Dq conditions. This temporal segregation indicates that C21 captures cells in acute (D0.01) versus consolidation (D3) phases of the transcriptional response, rather than representing a single stable neuronal population.

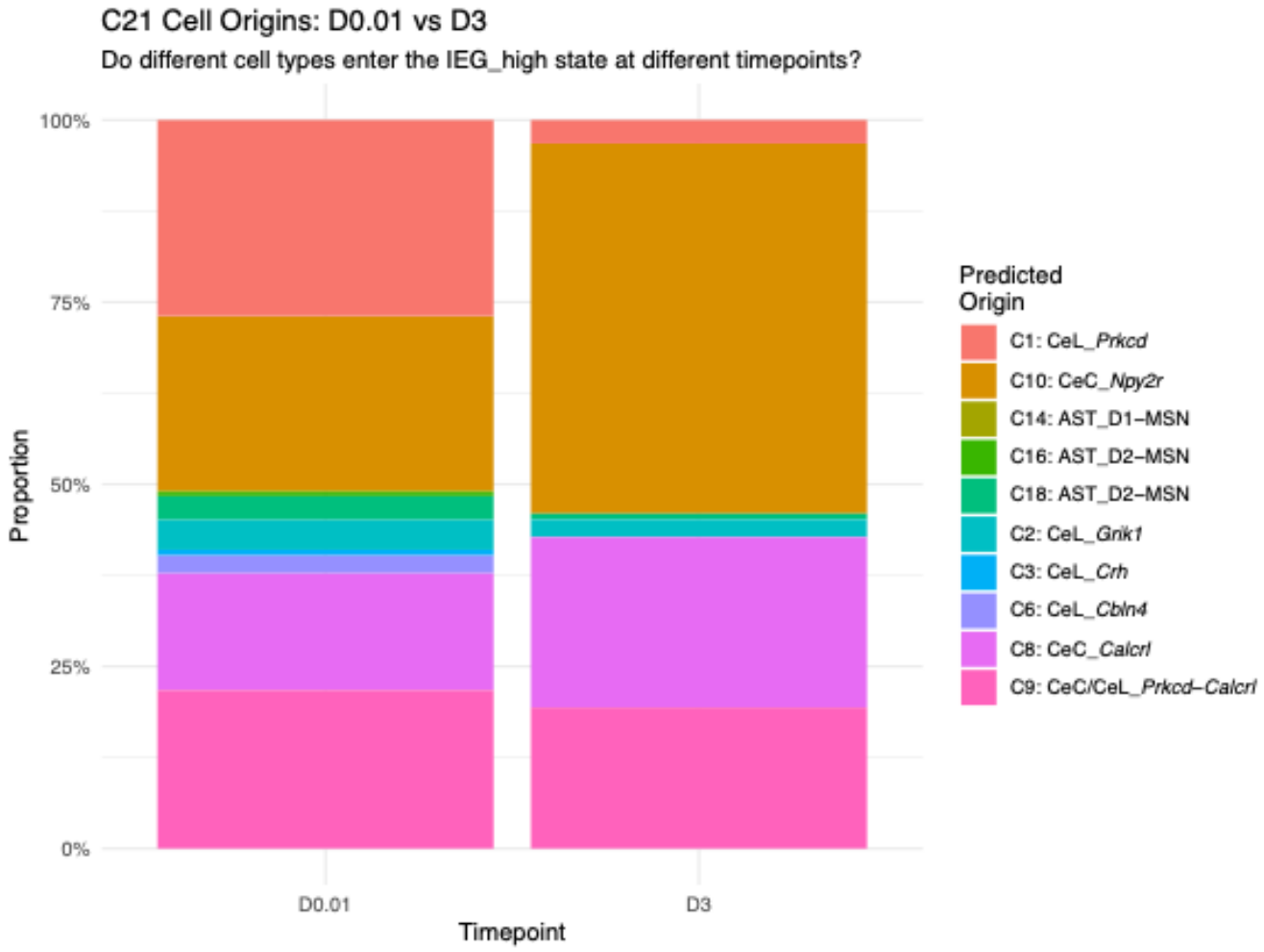

Figure 8. Temporal shift in C21 cell type origins between D0.01 and D3.

Stacked bar plot showing the predicted cell type origins of C21 (IEG_high) neurons at D0.01 (30 min) versus D3 (3 days) post-stimulation. At D0.01, C21 is predominantly composed of cells originating from C1 (CeL_*Prkcd*), consistent with the established role of *Prkcd* neurons in acute threat and pain responses. By D3, the composition shifts toward C10 (CeC_*Npy2r*) origin cells, suggesting preferential recruitment of *Npy2r* neurons during consolidation. This temporal shift in which cell types occupy the high-IEG state may reflect evolving circuit dynamics as acute nociceptive signaling transitions to longer-term plasticity processes.

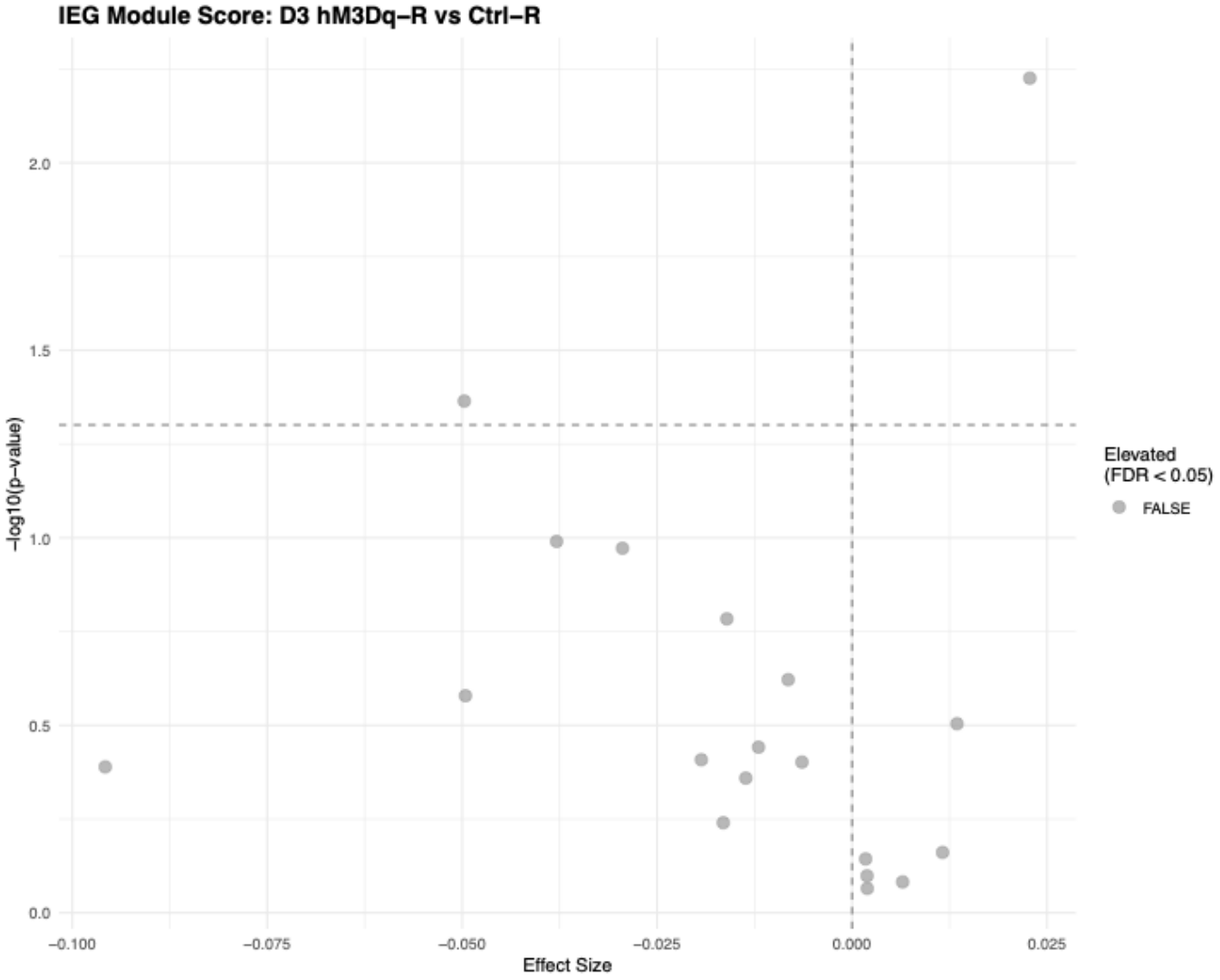

Figure 9. Acute IEG elevation resolves by D3.

Volcano plot showing IEG composite score effect sizes versus statistical significance for each cell type at D3 (3 days post-stimulation), comparing ipsilateral hemispheres between hM3Dq-treated and control animals. In contrast to robust acute responses at D0.01 (Figure 6), no cell types show significant IEG elevation at D3 (all FDR > 0.05). This indicates that the immediate transcriptional response to parabrachial *Calca* neuron activation is transient, resolving within 3 days. The absence of sustained IEG induction is consistent with these genes serving as acute activity markers rather than persistent plasticity indicators, though other consolidation-related transcriptional changes may occur independent of canonical IEG pathways.

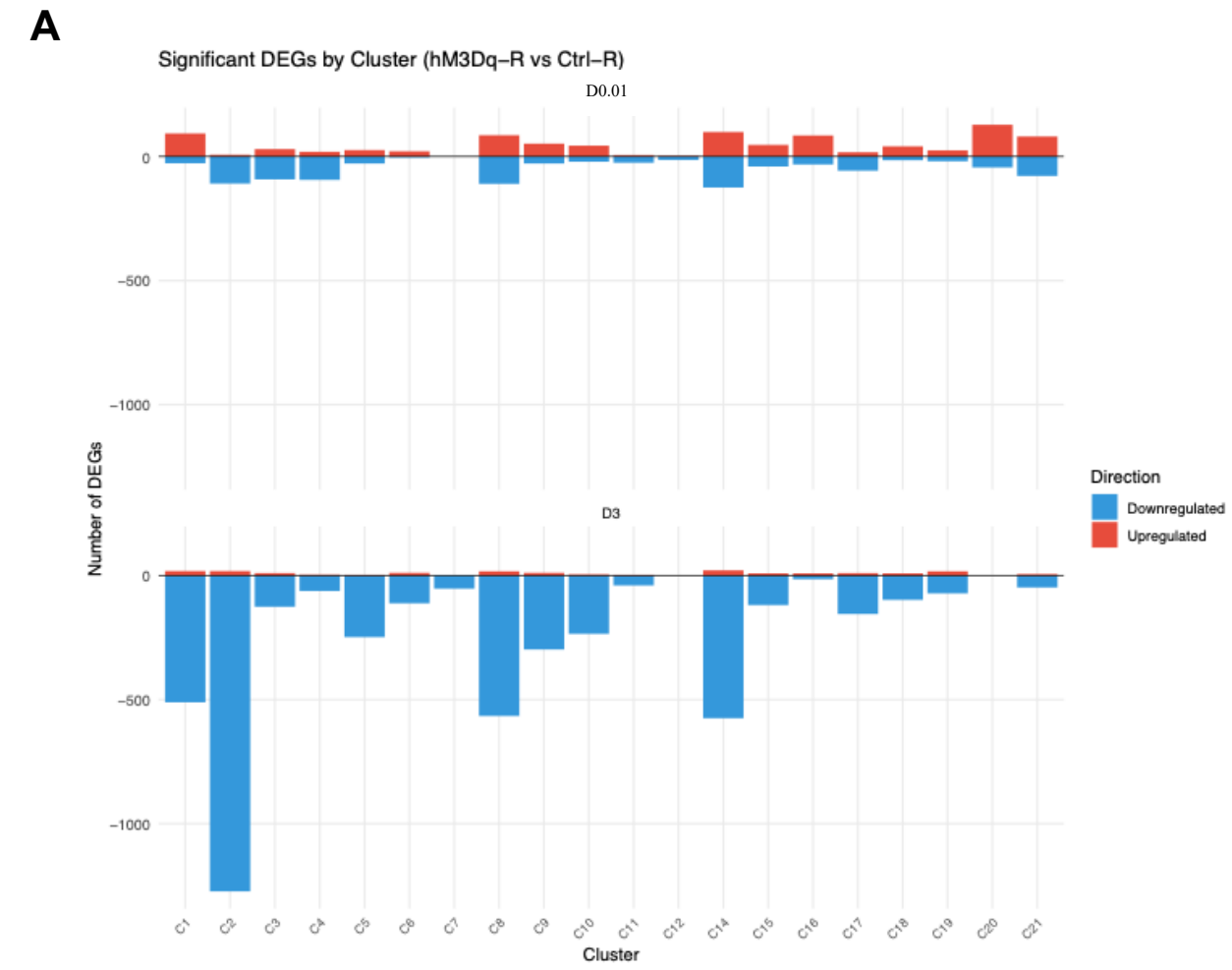

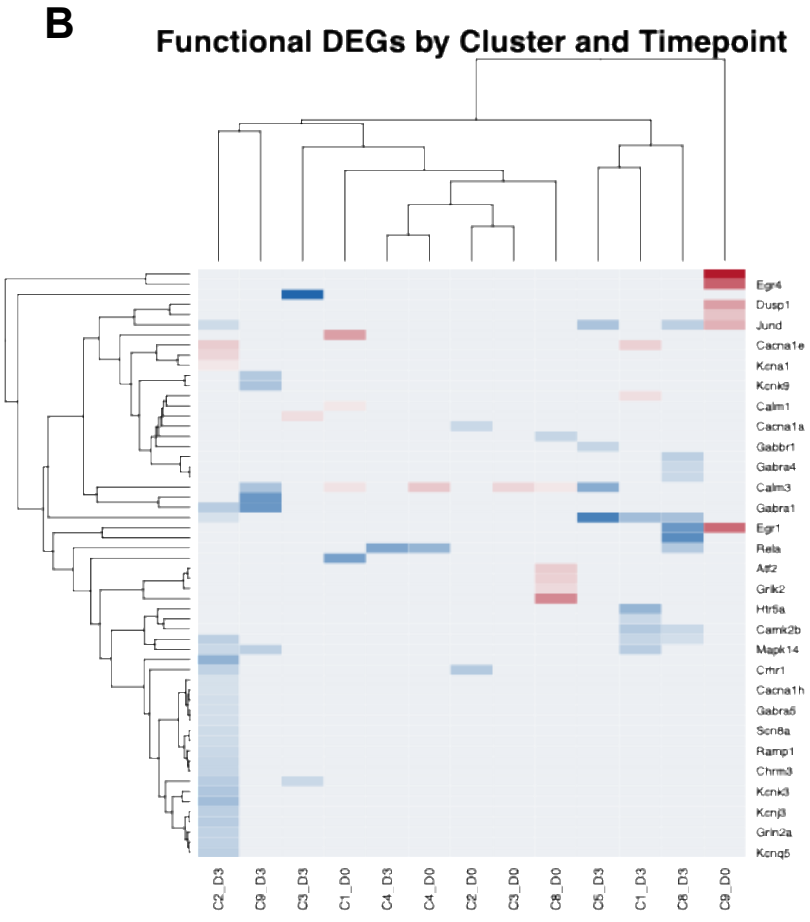

Figure 10. Differential gene expression overview across CeA clusters.

(A) Number of significant differentially expressed genes (DEGs; FDR < 0.05) per cluster at D0.01 (acute, 30 min post-injection) versus D3 (consolidation, 3 days post-injection). D3 shows substantially more DEGs across most clusters, with C2 (CeL_*Grik1*), C8 (CeC_*Calcrl*), and C1 (CeL_*Prkcd*) showing the largest expansions. (B) Breakdown of significant DEGs by functional category. Ion channels (30 vs 11), plasticity-related genes (28 vs 14), and transcription factors (13 vs 7) all show increased representation at D3, while canonical IEGs predominate at D0.01 (15 vs 10). DEGs were identified using Wilcoxon rank-sum tests comparing hM3Dq-treated versus control samples within the stimulated (right) hemisphere, with Benjamini-Hochberg correction for multiple testing.

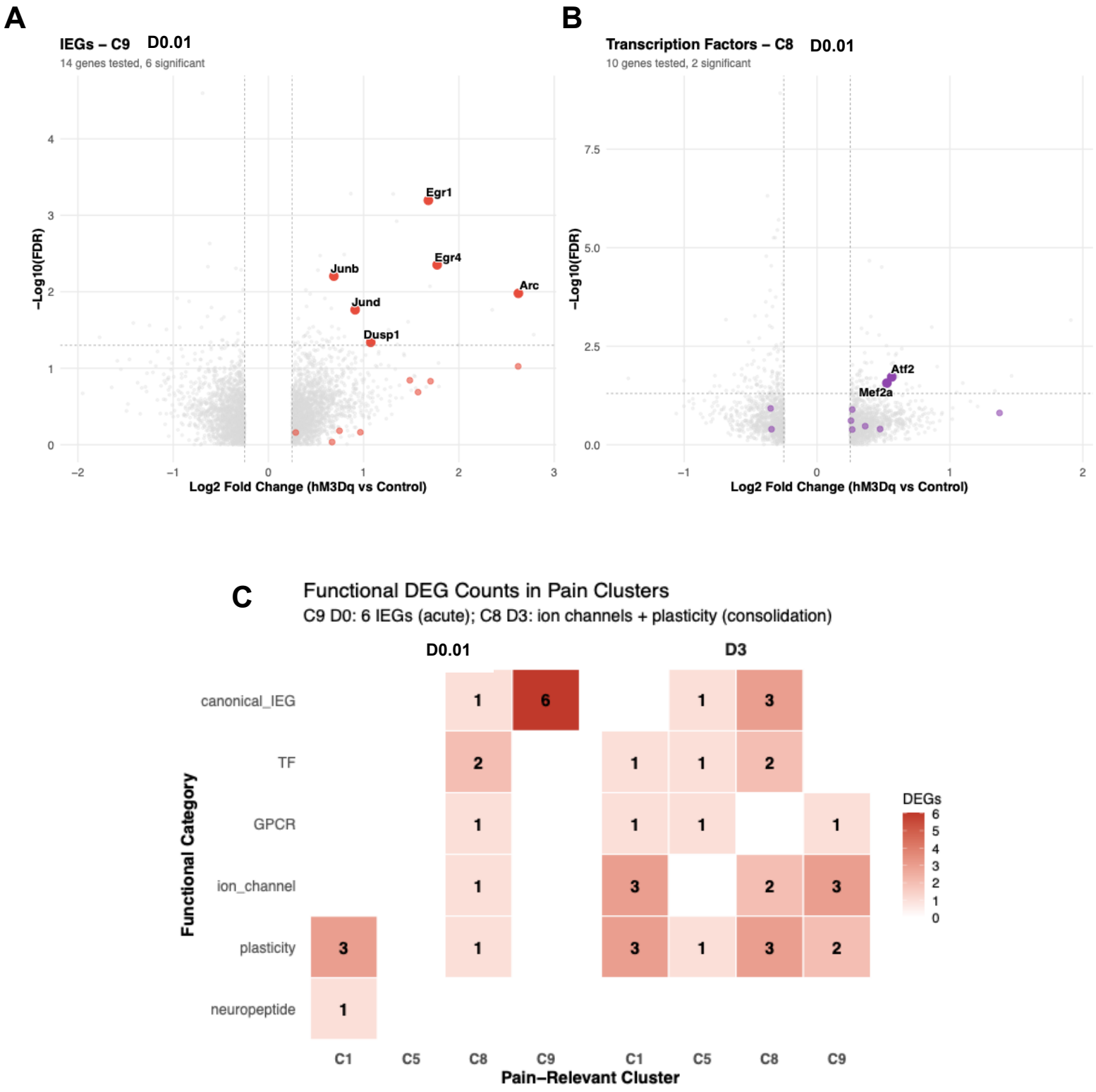

Figure 11. Acute transcriptional response in pain-relevant CeA clusters at D0.01.

(A) Volcano plot showing canonical immediate early genes (IEGs) in C9 (CeC/CeL_PKCd-Calcrl) at D0.01. Six IEGs reached significance (FDR < 0.05): *Egr1*, *Egr4*, *Junb*, *Arc*, *Jund*, and *Dusp1*, confirming acute activation of this *Calcrl/Prkcd* population following parabrachial stimulation. (B) Volcano plot showing transcription factors in C8 (CeC_Calcrl) at D0.01. Two activity-dependent TFs were significantly upregulated: *Atf2* and *Mef2a*, indicating early engagement of calcium/CREB-dependent transcriptional programs in CGRP-responsive neurons. (C) Heatmap summarizing functional DEG counts across pain-relevant clusters (C1: *Prkcd*, C5: *Sst*, C8: *Calcrl*, C9: *Prkcd/Calcrl*) at D0.01 versus D3. At D0.01, C9 shows the strongest acute response (6 IEGs); C8 shows TF and ion channel activation (*Grik2* upregulated); C1 shows calmodulin upregulation (*Calm1/2/3*) and *Tac1* downregulation. By D3, functional DEGs expand across all clusters with ion channels and plasticity genes predominating.

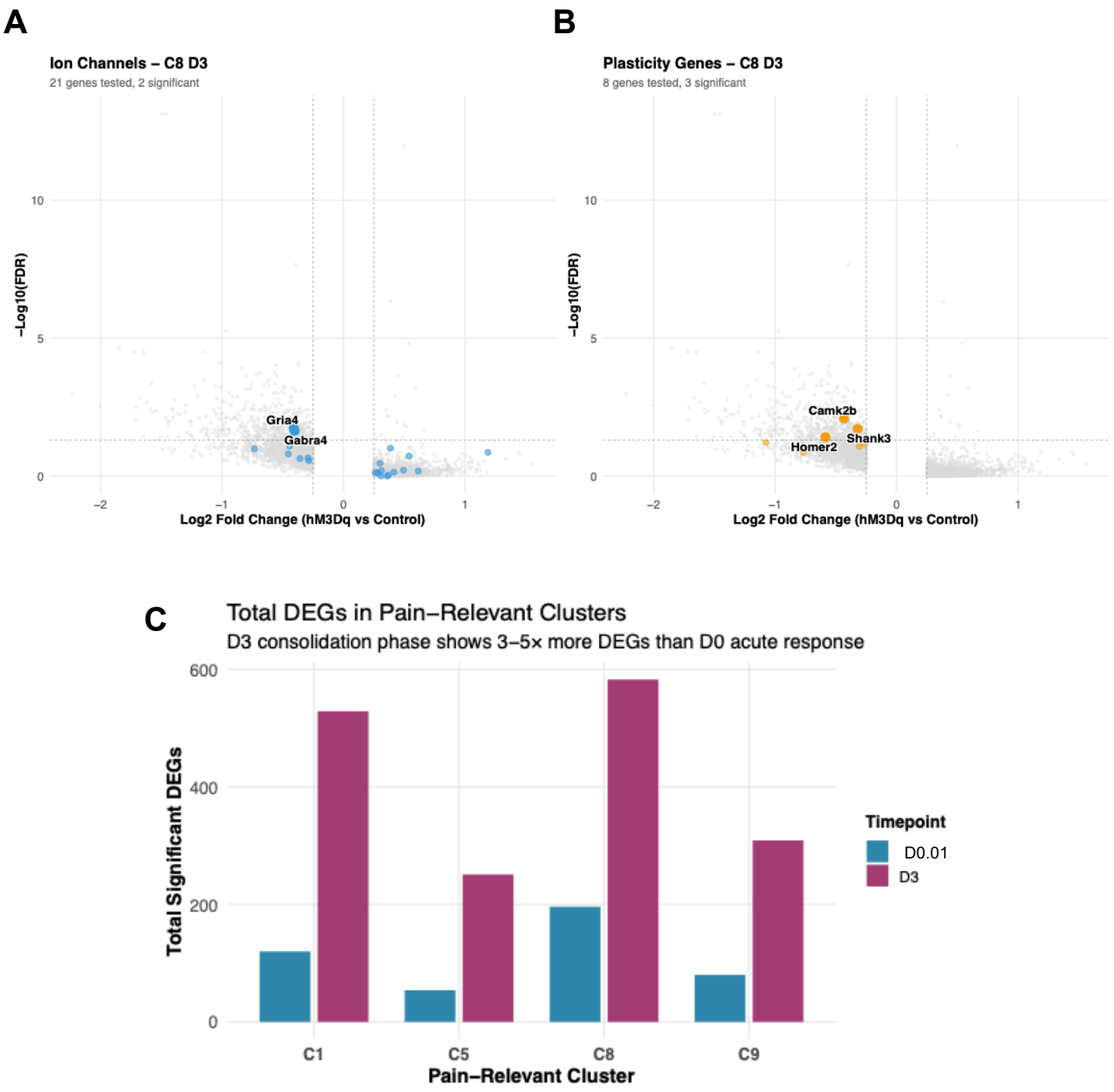

Figure 12. Consolidation-phase transcriptional remodeling in pain-relevant CeA clusters at D3.
(A) Volcano plot showing ion channel genes in C8 (CeC_Calcrl) at D3. Two ionotropic receptors were significantly downregulated: *Gria4* (AMPA receptor subunit GluA4) and *Gabra4* (GABA-A receptor α4 subunit), suggesting coordinated remodeling of excitatory and inhibitory synaptic transmission in CGRP-responsive neurons. (B) Volcano plot showing plasticity-related genes in C8 at D3. Three postsynaptic scaffolding components were significantly downregulated: *Camk2b* (CaMKII β subunit), *Shank3*, and *Homer2*, indicating structural reorganization of postsynaptic densities during the consolidation phase. (C) Total significant DEGs in pain-relevant clusters comparing D0.01 (acute) versus D3 (consolidation). All four clusters show 3-to 5-fold expansion in DEG counts at D3: C1 (120→529), C5 (54→251), C8 (196→583), and C9 (80→309). C8 (*Calcrl*) shows the largest absolute number of DEGs at both timepoints, consistent with its role as the primary recipient of parabrachial CGRP^{+} input. The predominance of downregulated genes at D3 suggests homeostatic scaling or synaptic refinement rather than simple potentiation.

Figure 13. Temporal dynamics of differential gene expression in CGRP-responsive CeA clusters. (A) Scatter plot comparing log2 fold change at D0.01 versus D3 for all tested genes in C8 (CeC_Calcrl). Of 196 DEGs at D0.01 and 583 at D3, only 15 genes showed sustained significance at both timepoints (e.g., *Syn2*, *Basp1*). The majority of D0.01 effects were acute-resolved (181 genes, including *Slc17a7*, *Dusp6*, *C1ql3*), while D3 showed 568 consolidation-emergent DEGs not detected acutely, predominantly downregulated (e.g., *Eef2*, *Egr3*, *Gstp1*). (B) Scatter plot for C9 (CeC/CeL_PKCd-Calcrl) showing even more distinct temporal separation. Of 80 DEGs at D0.01 and 309 at D3, only a single gene (*Tspoap1*) reached significance at both timepoints. Acute-resolved genes (79) included IEGs *Arc* and *Egr4*; consolidation-emergent genes (308) were predominantly downregulated. The minimal overlap between timepoints indicates that acute activation and consolidation-phase remodeling involve largely distinct transcriptional programs, rather than simple persistence or amplification of initial responses.

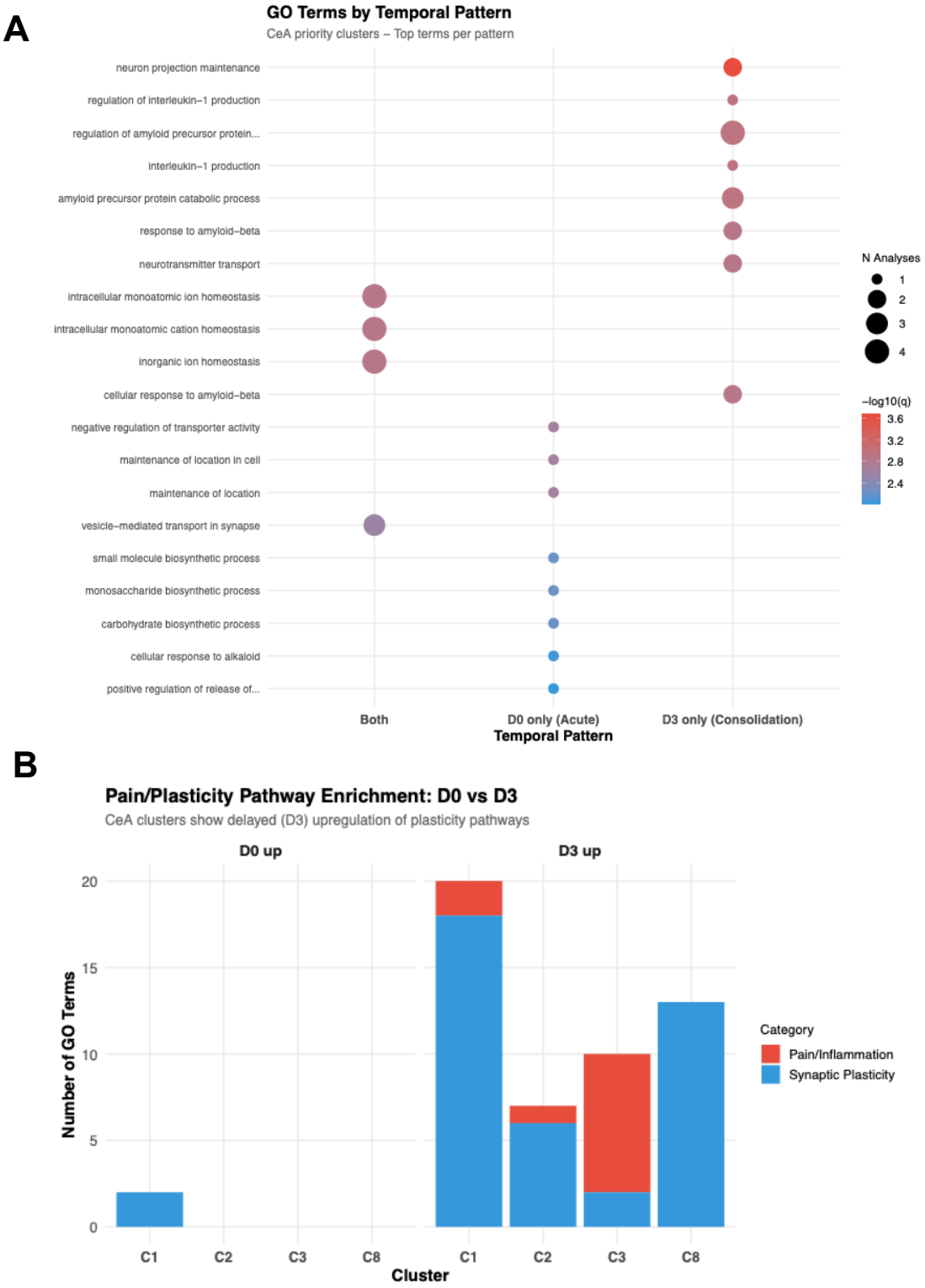

Figure 14. Gene ontology enrichment reveals consolidation-dominant pathway activation in CeA clusters. (A) Temporal distribution of enriched GO biological process terms. Of 253 significantly enriched terms across all clusters, 221 (87%) were specific to D3 (consolidation), only 28 (11%) were specific to D0.01 (acute), and 4 terms showed enrichment at both timepoints (including vesicle-mediated transport in synapse and ion homeostasis). D3-specific terms included neuron projection maintenance, neurotransmitter transport, cellular response to amyloid-beta, and regulation of synaptic transmission, consistent with active circuit remodeling rather than acute activation. D0.01-specific terms were largely metabolic (carbohydrate biosynthesis, maintenance of location). (B) Pain and plasticity-related GO terms in canonical CeA clusters. Of 52 total pain/plasticity terms enriched in CeA neurons (C1–C10), 50 appeared exclusively at D3 versus only 2 at D0.01, all in the upregulated direction. C8 (*Calcrl*) showed enrichment for dendritic spine maintenance, synaptic plasticity regulation, and signal release from synapse; C3 (*Crh*) showed cytokine production; C1 (*Prkcd*) showed positive regulation of synaptic transmission. This 25-fold enrichment of plasticity pathways at D3 versus D0.01 indicates that early consolidation, not acute activation, drives most pathway-level transcriptional reorganization in pain-relevant CeA populations.

IV. References

Allen, H. N., Bobnar, H. J., & Kolber, B. J. (2021). Left and right hemispheric lateralization of the amygdala in pain. *Progress in Neurobiology*, *196*, 101891. https://doi.org/10.1016/j.pneurobio.2020.101891

Allen, H. N., Chaudhry, S., Hong, V. M., Lewter, L. A., Sinha, G. P., Carrasquillo, Y., Taylor, B. K., & Kolber, B. J. (2023). A Parabrachial-to-Amygdala Circuit That Determines Hemispheric Lateralization of Somatosensory Processing. *Biological Psychiatry*, *93*(4), 370–381. https://doi.org/10.1016/j.biopsych.2022.09.010

Bonasera, S. J., Schenk, A. K., Luxenberg, E. J., Wang, X., Basbaum, A., & Tecott, L. H. (2015). Mice Lacking Serotonin 2C Receptors Have increased Affective Responses to Aversive Stimuli. *PLOS ONE*, *10*(12), e0142906. https://doi.org/10.1371/journal.pone.0142906

Bowen, A. J., Chen, J. Y., Huang, Y. W., Baertsch, N. A., Park, S., & Palmiter, R. D. (2020). Dissociable control of unconditioned responses and associative fear learning by parabrachial CGRP neurons. *eLife*, *9*, e59799. https://doi.org/10.7554/eLife.59799

Campos, C. A., Bowen, A. J., Roman, C. W., & Palmiter, R. D. (2018). Encoding of danger by parabrachial CGRP neurons. *Nature*, *555*(7698), 617–622. https://doi.org/10.1038/nature25511

Chen, J. Y., Campos, C. A., Jarvie, B. C., & Palmiter, R. D. (2018). Parabrachial CGRP Neurons Establish and Sustain Aversive Taste Memories. *Neuron*, *100*(4), 891-899.e5. https://doi.org/10.1016/j.neuron.2018.09.032

Choudhary, S., & Satija, R. (2022). Comparison and evaluation of statistical error models for scRNA-seq. *Genome Biology*, *23*(1), 27. https://doi.org/10.1186/s13059-021-02584-9

Ciocchi, S., Herry, C., Grenier, F., Wolff, S. B. E., Letzkus, J. J., Vlachos, I., Ehrlich, I., Sprengel, R., Deisseroth, K., Stadler, M. B., Müller, C., & Lüthi, A. (2010). Encoding of conditioned fear in central amygdala inhibitory circuits. *Nature*, *468*(7321), 277–282. https://doi.org/10.1038/nature09559

Condon, L. F., Yu, Y., Park, S., Cao, F., Pauli, J. L., Nelson, T. S., & Palmiter, R. D. (2024). Parabrachial Calca neurons drive nociplasticity. *Cell Reports*, *43*(4), 114057. https://doi.org/10.1016/j.celrep.2024.114057

Dedic, N., Kühne, C., Jakovcevski, M., Hartmann, J., Genewsky, A. J., Gomes, K. S., Anderzhanova, E., Pöhlmann, M. L., Chang, S., Kolarz, A., Vogl, A. M., Dine, J., Metzger, M. W., Schmid, B., Almada, R. C., Ressler, K. J., Wotjak, C. T., Grinevich, V., Chen, A., … Deussing, J. M. (2018). Chronic CRH depletion from GABAergic, long-range projection neurons in the extended amygdala reduces dopamine release and increases anxiety. *Nature Neuroscience*, *21*(6), 803–807. https://doi.org/10.1038/s41593-018-0151-z

Fadok, J. P., Krabbe, S., Markovic, M., Courtin, J., Xu, C., Massi, L., Botta, P., Bylund, K., Müller, C., Kovacevic, A., Tovote, P., & Lüthi, A. (2017). A competitive inhibitory circuit for selection of active and passive fear responses. *Nature*, *542*(7639), 96–100. https://doi.org/10.1038/nature21047

Fitzcharles, M.-A., Cohen, S. P., Clauw, D. J., Littlejohn, G., Usui, C., & Häuser, W. (2021). Nociplastic pain: Towards an understanding of prevalent pain conditions. *The Lancet*, *397*(10289), 2098–2110. https://doi.org/10.1016/S0140-6736(21)00392-5

Gandhi, P. J., Gawande, D. Y., Shelkar, G. P., Gakare, S. G., Kiritoshi, T., Ji, G., Misra, B., Pavuluri, R., Liu, J., Neugebauer, V., & Dravid, S. M. (2021). Dysfunction of Glutamate

Delta-1 Receptor-Cerebellin 1 Trans-Synaptic Signaling in the Central Amygdala in Chronic Pain. *Cells*, *10*(10), 2644. https://doi.org/10.3390/cells10102644

Germain, P.-L., Lun, A., Meixide, C. G., Macnair, W., & Robinson, M. D. (2022). *Doublet identification in single-cell sequencing data*.

Goto, F., Kiyama, Y., Ogawa, I., Okuno, H., Ichise, T., Ichise, H., Anai, M., Kodama, T., Yoshida, N., Bito, H., & Manabe, T. (2022). Gastrin-releasing peptide regulates fear learning under stressed conditions via activation of the amygdalostriatal transition area. *Molecular Psychiatry*, *27*(3), 1694–1703. https://doi.org/10.1038/s41380-021-01408-3

Guettier, J.-M., Gautam, D., Scarselli, M., De Azua, I. R., Li, J. H., Rosemond, E., Ma, X., Gonzalez, F. J., Armbruster, B. N., Lu, H., Roth, B. L., & Wess, J. (2009). A chemical-genetic approach to study G protein regulation of β cell function in vivo. *Proceedings of the National Academy of Sciences*, *106*(45), 19197–19202. https://doi.org/10.1073/pnas.0906593106

Han, J. S., Li, W., & Neugebauer, V. (2005). Critical Role of Calcitonin Gene-Related Peptide 1 Receptors in the Amygdala in Synaptic Plasticity and Pain Behavior. *The Journal of Neuroscience*, *25*(46), 10717–10728. https://doi.org/10.1523/JNEUROSCI.4112-05.2005

Han, S., Soleiman, M. T., Soden, M. E., Zweifel, L. S., & Palmiter, R. D. (2015). Elucidating an Affective Pain Circuit that Creates a Threat Memory. *Cell*, *162*(2), 363–374. https://doi.org/10.1016/j.cell.2015.05.057

Hao, Y., Stuart, T., Kowalski, M. H., Choudhary, S., Hoffman, P., Hartman, A., Srivastava, A., Molla, G., Madad, S., Fernandez-Granda, C., & Satija, R. (2024). Dictionary learning for integrative, multimodal and scalable single-cell analysis. *Nature Biotechnology*, *42*(2), 293–304. https://doi.org/10.1038/s41587-023-01767-y

Haubensak, W., Kunwar, P. S., Cai, H., Ciocchi, S., Wall, N. R., Ponnusamy, R., Biag, J., Dong, H.-W., Deisseroth, K., Callaway, E. M., Fanselow, M. S., Lüthi, A., & Anderson, D. J. (2010). Genetic dissection of an amygdala microcircuit that gates conditioned fear. *Nature*, *468*(7321), 270–276. https://doi.org/10.1038/nature09553

Hein, M., Ji, G., Tidwell, D., D'Souza, P., Kiritoshi, T., Yakhnitsa, V., Navratilova, E., Porreca, F., & Neugebauer, V. (2021). Kappa opioid receptor activation in the amygdala disinhibits CRF neurons to generate pain-like behaviors. *Neuropharmacology*, *185*, 108456. https://doi.org/10.1016/j.neuropharm.2021.108456

Hitchcock, J. M., & Davis, M. (1991). *Efferent Pathway of the Amygdala Involved in Conditioned Fear as Measured With the Fear-Potentiated Startle Paradigm*.

Hochgerner, H., Singh, S., Tibi, M., Lin, Z., Skarbianskis, N., Admati, I., Ophir, O., Reinhardt, N., Netser, S., Wagner, S., & Zeisel, A. (2023). Neuronal types in the mouse amygdala and their transcriptional response to fear conditioning. *Nature Neuroscience*, *26*(12), 2237–2249. https://doi.org/10.1038/s41593-023-01469-3

Ji, G., Zhang, W., Mahimainathan, L., Narasimhan, M., Kiritoshi, T., Fan, X., Wang, J., Green, T. A., & Neugebauer, V. (2017). 5-HT_{2C} Receptor Knockdown in the Amygdala Inhibits Neuropathic-Pain-Related Plasticity and Behaviors. *The Journal of Neuroscience*, *37*(6), 1378–1393. https://doi.org/10.1523/JNEUROSCI.2468-16.2016

Kato, F., Sugimura, Y. K., & Takahashi, Y. (2018). Pain-Associated Neural Plasticity in the Parabrachial to Central Amygdala Circuit: Pain Changes the Brain, and the Brain Changes the Pain. In B.-C. Shyu & M. Tominaga (Eds.), *Advances in Pain Research: Mechanisms and Modulation of Chronic Pain* (Vol. 1099, pp. 157–166). Springer Singapore. https://doi.org/10.1007/978-981-13-1756-9_14

Kim, J., Zhang, X., Muralidhar, S., LeBlanc, S. A., & Tonegawa, S. (2017). Basolateral to Central Amygdala Neural Circuits for Appetitive Behaviors. *Neuron*, *93*(6), 1464-1479.e5. https://doi.org/10.1016/j.neuron.2017.02.034

Kiritoshi, T., Yakhnitsa, V., Singh, S., Wilson, T. D., Chaudhry, S., Neugebauer, B., Torres-Rodriguez, J. M., Lin, J. L., Carrasquillo, Y., & Neugebauer, V. (2024). Cells and circuits for amygdala neuroplasticity in the transition to chronic pain. *Cell Reports*, *43*(9), 114669. https://doi.org/10.1016/j.celrep.2024.114669

Kissiwaa, S. A., & Bagley, E. E. (2018). Central sensitization of the spino-parabrachial-amygdala pathway that outlasts a brief nociceptive stimulus. *The Journal of Physiology*, *596*(18), 4457–4473. https://doi.org/10.1113/JP273976

Kosek, E., Cohen, M., Baron, R., Gebhart, G. F., Mico, J.-A., Rice, A. S. C., Rief, W., & Sluka, A. K. (2016). Do we need a third mechanistic descriptor for chronic pain states? *Pain*, *157*(7), 1382–1386. https://doi.org/10.1097/j.pain.0000000000000507

Kuner, R., & Kuner, T. (2021). Cellular Circuits in the Brain and Their Modulation in Acute and Chronic Pain. *Physiological Reviews*, *101*(1), 213–258. https://doi.org/10.1152/physrev.00040.2019

Latremoliere, A., & Woolf, C. J. (2009). Central Sensitization: A Generator of Pain Hypersensitivity by Central Neural Plasticity. *The Journal of Pain*, *10*(9), 895–926. https://doi.org/10.1016/j.jpain.2009.06.012

LeDoux, J., Iwata, J., Cicchetti, P., & Reis, D. (1988). Different projections of the central amygdaloid nucleus mediate autonomic and behavioral correlates of conditioned fear. *The Journal of Neuroscience*, *8*(7), 2517–2529. https://doi.org/10.1523/JNEUROSCI.08-07-02517.1988

Manvich, D. F., Webster, K. A., Foster, S. L., Farrell, M. S., Ritchie, J. C., Porter, J. H., & Weinshenker, D. (2018). The DREADD agonist clozapine N-oxide (CNO) is reverse-metabolized to clozapine and produces clozapine-like interoceptive stimulus effects in rats and mice. *Scientific Reports*, *8*(1), 3840. https://doi.org/10.1038/s41598-018-22116-z

Mazzitelli, M., Marshall, K., Pham, A., Ji, G., & Neugebauer, V. (2021). Optogenetic Manipulations of Amygdala Neurons Modulate Spinal Nociceptive Processing and Behavior Under Normal Conditions and in an Arthritis Pain Model. *Frontiers in Pharmacology*, *12*, 668337. https://doi.org/10.3389/fphar.2021.668337

Neugebauer, V., Li, W., Bird, G. C., & Han, J. S. (2004). The Amygdala and Persistent Pain. *The Neuroscientist*, *10*(3), 221–234. https://doi.org/10.1177/1073858403261077

O'Leary, T. P., Kendrick, R. M., Bristow, B. N., Sullivan, K. E., Wang, L., Clements, J., Lemire, A. L., & Cembrowski, M. S. (2022). Neuronal cell types, projections, and spatial organization of the central amygdala. *iScience*, *25*(12), 105497. https://doi.org/10.1016/j.isci.2022.105497

Palmiter, R. D. (2018). The Parabrachial Nucleus: CGRP Neurons Function as a General Alarm. *Trends in Neurosciences*, *41*(5), 280–293. https://doi.org/10.1016/j.tins.2018.03.007

Palmiter, R. D. (2024). Parabrachial neurons promote nociplastic pain. *Trends in Neurosciences*, *47*(9), 722–735. https://doi.org/10.1016/j.tins.2024.07.002

Park, S., Zhu, A., Cao, F., & Palmiter, R. D. (2024). Parabrachial Calca neurons mediate second-order conditioning. *Nature Communications*, *15*(1), 9721. https://doi.org/10.1038/s41467-024-53977-w

Pauli, J. L., Chen, J. Y., Basiri, M. L., Park, S., Carter, M. E., Sanz, E., McKnight, G. S., Stuber, G. D., & Palmiter, R. D. (2022). Molecular and anatomical characterization of

parabrachial neurons and their axonal projections. *eLife*, *11*, e81868. https://doi.org/10.7554/eLife.81868

Phelps, C. E., Navratilova, E., Dickenson, A. H., Porreca, F., & Bannister, K. (2019). Kappa opioid signaling in the right central amygdala causes hind paw specific loss of diffuse noxious inhibitory controls in experimental neuropathic pain. *Pain*, *160*(7), 1614–1621. https://doi.org/10.1097/j.pain.0000000000001553

Phipson, B., Sim, C. B., Porrello, E. R., Hewitt, A. W., Powell, J., & Oshlack, A. (2022). *propeller: Testing for differences in cell type proportions in single cell data*.

Pitkänen, A., Savander, V., & LeDoux, J. E. (1997). Organization of intra-amygdaloid circuitries in the rat: An emerging framework for understanding functions of the amygdala. *Trends in Neurosciences*, *20*(11), 517–523. https://doi.org/10.1016/S0166-2236(97)01125-9

Pomrenze, M. B., Giovanetti, S. M., Maiya, R., Gordon, A. G., Kreeger, L. J., & Messing, R. O. (2019). Dissecting the Roles of GABA and Neuropeptides from Rat Central Amygdala CRF Neurons in Anxiety and Fear Learning. *Cell Reports*, *29*(1), 13-21.e4. https://doi.org/10.1016/j.celrep.2019.08.083

Presto, P., & Neugebauer, V. (2022). Sex Differences in CGRP Regulation and Function in the Amygdala in a Rat Model of Neuropathic Pain. *Frontiers in Molecular Neuroscience*, *15*, 928587. https://doi.org/10.3389/fnmol.2022.928587

Raver, C., Uddin, O., Ji, Y., Li, Y., Cramer, N., Jenne, C., Morales, M., Masri, R., & Keller, A. (2020). An Amygdalo-Parabrachial Pathway Regulates Pain Perception and Chronic Pain. *The Journal of Neuroscience*, *40*(17), 3424–3442. https://doi.org/10.1523/JNEUROSCI.0075-20.2020

Rizvi, T. A., Ennis, M., Behbehani, M. M., & Shipley, M. T. (1991). Connections between the central nucleus of the amygdala and the midbrain periaqueductal gray: Topography and reciprocity. *Journal of Comparative Neurology*, *303*(1), 121–131. https://doi.org/10.1002/cne.903030111

Sah, P., Faber, E. S. L., Lopez De Armentia, M., & Power, J. (2003). The Amygdaloid Complex: Anatomy and Physiology. *Physiological Reviews*, *83*(3), 803–834. https://doi.org/10.1152/physrev.00002.2003

Sanford, C. A., Soden, M. E., Baird, M. A., Miller, S. M., Schulkin, J., Palmiter, R. D., Clark, M., & Zweifel, L. S. (2017). A Central Amygdala CRF Circuit Facilitates Learning about Weak Threats. *Neuron*, *93*(1), 164–178. https://doi.org/10.1016/j.neuron.2016.11.034

Swanson, L. W., & Petrovich, G. D. (1998). What is the amygdala? *Trends in Neurosciences*, *21*(8), 323–331. https://doi.org/10.1016/S0166-2236(98)01265-X

Tasan, R. O., Verma, D., Wood, J., Lach, G., Hörmer, B., De Lima, T. C. M., Herzog, H., & Sperk, G. (2016). The role of Neuropeptide Y in fear conditioning and extinction. *Neuropeptides*, *55*, 111–126. https://doi.org/10.1016/j.npep.2015.09.007

Verma, D., Wood, J., Lach, G., Mietzsch, M., Weger, S., Heilbronn, R., Herzog, H., Bonaventure, P., Sperk, G., & Tasan, R. O. (2015). NPY Y2 receptors in the central amygdala reduce cued but not contextual fear. *Neuropharmacology*, *99*, 665–674. https://doi.org/10.1016/j.neuropharm.2015.08.038

Wang, Y., Krabbe, S., Eddison, M., Henry, F. E., Fleishman, G., Lemire, A. L., Wang, L., Korff, W., Tillberg, P. W., Lüthi, A., & Sternson, S. (2023). Multimodal mapping of cell types and projections in the central nucleus of the amygdala. *eLife*, *12*, e84262. https://doi.org/10.7554/eLife.84262

Wilson, T. D., Valdivia, S., Khan, A., Ahn, H.-S., Adke, A. P., Martinez Gonzalez, S., Sugimura, Y. K., & Carrasquillo, Y. (2019). Dual and Opposing Functions of the Central Amygdala in the Modulation of Pain. *Cell Reports*, *29*(2), 332-346.e5. https://doi.org/10.1016/j.celrep.2019.09.011

Woolf, C. J. (2011). Central sensitization: Implications for the diagnosis and treatment of pain. *Pain*, *152*(3), S2–S15. https://doi.org/10.1016/j.pain.2010.09.030

Yao, Z., Van Velthoven, C. T. J., Kunst, M., Zhang, M., McMillen, D., Lee, C., Jung, W., Goldy, J., Abdelhak, A., Aitken, M., Baker, K., Baker, P., Barkan, E., Bertagnolli, D., Bhandiwad, A., Bielstein, C., Bishwakarma, P., Campos, J., Carey, D., … Zeng, H. (2023). A high-resolution transcriptomic and spatial atlas of cell types in the whole mouse brain. *Nature*, *624*(7991), 317–332. https://doi.org/10.1038/s41586-023-06812-z

Yeh, L.-F., Zuo, S., & Liu, P.-W. (2024). Molecular diversity and functional dynamics in the central amygdala. *Frontiers in Molecular Neuroscience*, *17*, 1364268. https://doi.org/10.3389/fnmol.2024.1364268

Yu, B., Zhang, Q., Lin, L., Zhou, X., Ma, W., Wen, S., Li, C., Wang, W., Wu, Q., Wang, X., & Li, X.-M. (2023). Molecular and cellular evolution of the amygdala across species analyzed by single-nucleus transcriptome profiling. *Cell Discovery*, *9*(1), 19. https://doi.org/10.1038/s41421-022-00506-y

Zimmerman, C. A., Bolkan, S. S., Pan-Vazquez, A., Wu, B., Keppler, E. F., Meares-Garcia, J. B., Guthman, E. M., Fetcho, R. N., McMannon, B., Lee, J., Hoag, A. T., Lynch, L. A., Janarthanan, S. R., López Luna, J. F., Bondy, A. G., Falkner, A. L., Wang, S. S.-H., & Witten, I. B. (2023). *A neural mechanism for learning from delayed postingestive feedback*. https://doi.org/10.1101/2023.10.06.561214